https://ntrs.nasa.gov/search.jsp?R=19740023304 2020-03-23T03:57:15+00:00Z

NASA TECHNICAL MEMORANDUM

NASA TM X-3042

NASA TM X-3042

TRANSONIC OFF-DESIGN DRAG AND PERFORMANCE OF AN AXISYMMETRIC INLET WITH 40-PERCENT INTERNAL CONTRACTION ON DESIGN

by Richard R. Woollett, Edward T. Meleason, and David A. Choby

Lewis Research Center
Cleveland, Ohio 44135

NATIONAL AERONAUTICS AND SPACE ADMINISTRATION • WASHINGTON, D. C. • AUGUST 1974

1. Report No.	2. Government Accession No.	3. Recipient's Catalog No.
NASA TM X-3042		

4. Title and Subtitle	5. Report Date
TRANSONIC OFF-DESIGN DRAG AND PERFORMANCE OF AN AXISYMMETRIC INLET WITH 40-PERCENT INTERNAL CONTRACTION ON DESIGN	AUGUST 1974
	6. Performing Organization Code
7. Author(s)	8. Performing Organization Report No.
Richard R. Woollett, Edward T. Meleason, and David A. Choby	E-7692
	10. Work Unit No.
9. Performing Organization Name and Address	501-24
Lewis Research Center National Aeronautics and Space Administration Cleveland, Ohio 44135	11. Contract or Grant No.
	13. Type of Report and Period Covered
12. Sponsoring Agency Name and Address	Technical Memorandum
National Aeronautics and Space Administration Washington, D.C. 20546	14. Sponsoring Agency Code

15. Supplementary Notes

16. Abstract

An experimental investigation determined the drag and pressure performance of an axisymmetric supersonic inlet when operated in the transonic speed range. The inlet configuration was derived from a Mach 2.5 mixed compression inlet design with assumed variable geometry. At typical engine airflows the drag coefficient varied from 0.057 to 0.192 when the Mach number changed from 0.80 to 1.27. The presence of a wing simulator resulted in a sizable increase in total drag at Mach 1.2. This interference drag, which is roughly a 0.1 increase in drag coefficient, originates equally from an increase in both additive and cowl pressure drag.

17. Key Words (Suggested by Author(s))	18. Distribution Statement
Drag; Transonic; Supersonic inlet; Installation drag; Off-design inlet	Unclassified - unlimited CAT. 01

19. Security Classif. (of this report)	20. Security Classif. (of this page)	21. No. of Pages	22. Price*
Unclassified	Unclassified	54	$3.75

* For sale by the National Technical Information Service, Springfield, Virginia 22151

TRANSONIC OFF-DESIGN DRAG AND PERFORMANCE OF AN AXISYMMETRIC INLET WITH 40-PERCENT INTERNAL CONTRACTION ON DESIGN

by Richard R. Woollett, Edward T. Meleason, and David A. Choby
Lewis Research Center

SUMMARY

An experimental investigation was conducted to determine the drag and pressure performance of an axisymmetric supersonic inlet when operated off design in the transonic speed range. The inlet configuration was derived from a Mach 2.5 mixed compression inlet design with assumed variable geometry.

At typical engine airflows the drag coefficient varied from 0.057 to 0.192 when the Mach number changed from 0.80 to 1.27. In general, the drag characteristics of the inlet including additive and cowl pressure drag exhibited the typical drag rise associated with slender bodies or wings. Below Mach number 0.90 a lower drag result when the excess airflow is spilled over the cowl rather than through the bypass doors: above Mach number 1.1 it is best to spill only 20 to 25 percent of the excess flow through the bypass doors.

The presence of a wing simulator resulted in a sizable increase in total drag at Mach 1.2. This interference drag, which is roughly a 0.1 increase in drag coefficient (based on inlet capture area), originates equally from an increase in both additive and cowl pressure drag. At lower Mach numbers the wing had very little influence on the total drag.

Generally, configurations using single flap bypass doors gave larger drags than those using multiple flap doors. The largest difference in drag coefficient was 0.02; this difference occurred at a free stream Mach number of 1.27 and bypass flap angle of 10^{o}.

INTRODUCTION

When supersonic inlets are flown at transonic speeds, the engine requires only about 60 percent of the capture mass flow. The manner in which the excess mass flow is spilled affects the drag of the nacelle. It has been estimated that the drag penalty

associated with spilling this air on a Mach 2.7 transport can be as much as 3 percent of the payload, even though it occurs only during acceleration and deceleration of the vehicle through the sonic region (ref. 1). If a holding pattern is required, the additional fuel needed will depend directly on the subsonic drag and consequently on how the excess air is dumped. The fuel required for the subsonic part of a typical mission plus a reserve required for a possible holding pattern can easily be equal to the weight of the payload (ref. 2). Moreover, this does not include any fuel for a flight pattern over land that may limit the aircraft to subsonic speeds. Consequently, any improvements in subsonic and transonic drag can significantly affect the payload.

The NASA Lewis Research Center is conducting tests to evaluate the performance characteristics of a series of supersonic inlets at off-design conditions. The present report presents data of one axisymmetric inlet that was tested under this program. At the inlet design Mach number of 2.5, 40 percent of the supersonic area contraction was internal. The design configuration of the mixed compression inlet was previously tested at Mach 2.5 (ref. 3). The off-design configuration was formed by collapsing the throat region of the centerbody surface and translating the centerbody forward to eliminate internal contraction. These modifications of the on-design inlet would provide adequate weight flow for a typical turbojet engine during transonic operation.

There are several ways in which spilled air can be handled with fixed cowl inlets: (1) air can be dumped over the cowl, or (2) it can be taken on board and then dumped through bypass doors ahead of the compressor face station. When air is dumped over the cowl, a favorable cowl suction force exists. Just when it is best to bypass the flow varies with the individual inlet and flight Mach number. The present report evaluates the various schemes to dump the excess air and includes a relative evaluation of multiple and single flap bypass doors.

The transonic performance including compressor face total pressure recovery, steady-state distortion, dynamic distortion, and cowl, spike, and wing surface static pressures is presented. In addition, total drag measurements were taken. The drag is broken into its various components, that is, additive, cowl, and friction. The influence of a nearby simulated wing is also investigated.

The tests were conducted in the Lewis Research Center 8 by 6 Foot Supersonic Wind Tunnel over a Mach range of 0.8 to 1 27. For the 25.4-centimeter model tested, the inlet Reynolds number was roughly 3.7×10^6. Although U.S. Customary Units were specified when the model was fabricated, all the dimensions reported herein are either in SI Units or are nondimensional. The definitions of the symbols used in this report are presented in appendix A.

APPARATUS AND PROCEDURE

Model

The basic inlet coordinates were obtained by modifying the coordinates of a double cone inlet tested earlier at Mach 2.5 (ref. 3) to eliminate all internal contraction. The supersonic area contraction of a capture stream tube of the design inlet was 60 percent external and 40 percent internal. The centerbody surface was changed to simulate a configuration that would result if the surfaces of the design inlet were collapsed to lower the 18° half angle of the second cone to the 10° value of the first cone. In addition, it was necessary to translate the entire centerbody upstream to achieve the aforementioned transonic design criteria of no internal contraction. The configuration will hereafter be referred to as the 60-40 T inlet, where the T means translated. The surface coordinates and the area variation of both the design and transonic version of the 60-40 T inlet are plotted in figure 1. Table I lists the nondimensional coordinates of the external surfaces of the inlet from the cone tip of the centerbody downstream to the compressor face station. The upstream opening of the bypass doors is 3.619 and the downstream opening is 4.061 cowl diameters from the centerbody tip of the inlet. The centerbody has been translated 0.291 cowl diameter upstream. The capture area of the inlet is 375.8 square centimeters (58.25 in.^{2}).

A schematic drawing showing the cross section of the model is presented in figure 2(a). With the exception of the model support sting, the mass flow exit plug, and the outer shell windshield and base pressure skirt, the entire model formed the metric unit of the force measuring system. The outer shell windshield and base pressure skirt were grounded in the force system in the axial direction but were free to move in the transverse direction. This type of constraint would eliminate any excessive perpendicular forces due to model deflections. These nonmetric parts of the model are identified in the schematic presented in figure 2(a). The nonmetric outer shell windshield was used to reduce the friction drag over the aft part of the model. A bearing of 30 Teflon spacers was installed between the outer shield and the 25.4-centimeter metric cylinder. These triangular shaped spacers prevent the friction drag from being transferred to the metric cylinder (see fig. 2(c)). To prevent air flow between the two surfaces and a resulting friction drag, a neoprene curtain was installed in the annular passage between the two shells near the leading edge of the outer shell windshield.

The load cell mounted between the centerbody and model support sting (fig. 2(a)) had a load capacity of ±4448 newtons. Since variations in perpendicular loads affect the load cell reading, the load cell has to be isolated from all such forces. Both a sting bearing and a strut bearing (fig. 2(b)) were used to isolate the perpendicular loads on the load cell. If the strut bearing had not been used, the estimated perpendicular loads on the sting bearing would have exceeded their design limits. The side forces were eliminated

by using the bearing parts of a separate strut balance system in which the strain gages were removed. This bearing system removed both vertical and horizontal forces so that only axial forces were actually applied to the load cell. The maximum deviation of the load cell was less than ±6.7 newtons from the linear calibration curve used in this test.

Five bypass door configurations were tested: (1) closed bypass doors, which are indicated by the dotted line in figure 3(a); (2) 5° single flap bypass doors, which are depicted in figure 3(a); (3) 10° single flap bypass doors; (4) 5° multiple flap bypass doors; and (5) 10° multiple bypass doors, which are depicted in figure 3(b). The flow passage between each of the flaps has side plates in order to eject the bypass flow mainly in a downstream direction. The actual detail of the flap construction is depicted in figure 3(c). The general location of the door with respect to the inlet can be seen in the model schematic of figure 2(a) which depicts the 5° multiple flap bypass door configuration. Photographs of the 10° single and multiple flap door showing upstream and downstream views, respectively, are shown in figures 4 and 5. In figure 5 a spare multiple flap door insert is setting on top of the model to present an underside view of the bypass doors.

A portion of the inlet performance and drag tests was run with the nacelle under a flat plate set at a 0° angle of attack. This flat plate simulated a wing in order to evaluate the installation drag associated with an underwing nacelle installation. The leading edge of the plate is located 5.4 cowl diameters upstream of the cowl lip. The cowl lip of the inlet is positioned nominally 0.21 cowl diameter below the plate. The total length of the flat plate is 7.9 cowl diameters. A photograph of the nacelle mounted under the wing simulator is presented in figure 6.

Instrumentation

The testing was divided into two parts: one was primarily concerned with the bulk of pressure measurement, and the other was primarily concerned with the force measurements of the load cell. This split in data taking was necessary because a large bundle of pressure tubes spanned the balance in a rather confined space. Duplicate runs were made for each bypass door configuration, and the measurements were correlated by the measured mass flow at the exit plug. Consequently, when the drag and performance of one inlet configuration was compared with another configuration it was necessary first to plot the data as functions of mass flow m_3/m_0 in order to obtain a commonality of test conditions.

The pressure measurements included an axial row of static pressures along the centerbody at 90° and along the top (0°) external surface of the cowl. The locations of these static pressure taps are listed in table II and their relative positioning on the inlet is shown in figure 7. The total and static pressure instrumentation located at the

compressor face station is depicted in figure 7(b). There are five 6-tube total pressure rakes, one 4-tube dynamic pressure rake, and 9 wall statics at this model station. There are total rakes located at the same circumferential angle as the centerline of the bypass doors as well as midway between the bypass doors. These doors are just upstream of the rakes (fig. 3). Total pressures are measured at the cowl face station with a single rake as depicted in figure 7(c). The positioning of all total pressure tubes are area weighted for the flow passage where they are located. In addition, wing static (fig. 7(a)) and mass flow static pressures were recorded. Base static pressures and load cell chamber pressure were also taken in order to calculate tare loads (see appendix B). The definition of the drag terms along with the derivation of the equations used to obtain the additive and total inlet drag from measured quantities are also presented in appendix B.

The dynamic pressures were recorded with subminiature strain gage type pressure transducers whose output was fed into rms meters. The values of dynamic distortion reported herein are area weighted averages of the four dynamic total pressures taken at the compressor face station. The bypass mass flow ratio m_{bp}/m_0 is obtained by subtracting compressor face mass flow ratios measured at a particular open bypass condition from that measured with closed bypass door at the same cowl-lip-station entrance Mach number M_1. The entrance Mach number is determined by using an average area weighted total pressure from the cowl face rake and the centerbody static pressures measured at the rake station.

The axial loads reported are an average of 10 readings randomly taken over a period of roughly 2 seconds. This technique of data taking was necessitated by a condition of model vibration during testing and resulted in typical standard deviations of the 10 load cell readings of 8 newtons.

Test Condition

The Mach numbers tested were nominally 0.8, 0.9, 1.0, 1.1, 1.2, and 1.27. The associated Reynolds numbers were roughly 1.38, 1.41, 1.46, 1.51, 1.54, and 1.54×10^7 per meter, respectively. The inlet nacelle was tested both under a wing and isolated without a wing. During the isolated nacelle test, the inlet was tested at angles of attack of 2°, 5°, and 10° at Mach 1.27 and at 0° at all six Mach numbers. The engine corrected weight flow schedule used herein is presented in figure 8.

RESULTS AND DISCUSSION

The total drag coefficient and performance of the 60-40 T inlet at the design corrected weight flow are plotted as functions of Mach number for two bypass door configurations in figure 9. The experimental data were cross-plotted to obtain the curve. There are transonic drag rises of roughly 0.140 and 0.100 in the total drag coefficient associated with the closed and 5° flap bypass door configurations, respectively. The major part of the drag rise lies between Mach 0.9 and 1.1. At a free stream Mach number of 0.8 there are lower total drags with cowl spillage (bypass closed) than with the bypass spillage configurations (5° bypass door configuration). At a free stream Mach number of 1.27 the opposite is true and the bypass spillage configurations have a lower drag than cowl spillage configurations. When single flap doors were installed in place of the multiple flap doors the total drag coefficient at subsonic speeds increased by at most 0.015.

The transonic no bypass flow total pressure recovery of the 60-40 T inlet measured at the design corrected weight flow was 0.984 at Mach 0.8 and varied only 0.005 between Mach 0.8 and 1.2. However, at Mach 1.27 the recovery is starting to drop faster, the drop being 0.005 between 1.2 and 1.27. When the multiple flap bypass doors are set at 5° the total pressure drop of 0.005 at Mach 1.27 is not observed (see fig. 9(b)).

The inlet exhibited a steady-state distortion value that lies within the 0.06 to 0.11 range at design corrected weight flow. There is a greater percentage difference in the steady-state distortion and dynamic distortion between the two bypass configurations than experienced with the total pressure recovery. Not only is the steady-state distortion 0.02 to 0.03 count larger when 5° flap doors are used, but it is also not constant over the Mach number range tested (see fig. 9). The magnitudes of the dynamic distortion data are relatively low and consequently may not be of much interest. The dynamic distortion for both bypass conditions falls mostly in the 0.005 to 0.009 range. At no condition was the distortion outstandingly better or poorer than any other condition. The experimental data of total pressure recovery, steady-state distortion, dynamic distortion, and total drag coefficient over a range of mass flow ratio are presented for reference only in figures 23, 24, and 25.

The wing installation effect on the 60-40 T inlet results in an increase of the total inlet drag coefficient of roughly 0.1 at Mach 1.27 with and without bypass. These wing installation results are also presented in figures 9(a) and (b). It can be seen that there is very little effect of the presence of the wing on the total pressure recovery and dynamic distortion of the bypass door 5° flap configuration. The raw data of total pressure recovery, steady-state distortion, dynamic distortion, and total drag coefficient over a range of mass flow ratios with a nacelle under a wing are presented in figures 24 and 25.

Inlet Performance

Angle of attack. - Angle of attack data at a free stream Mach number of 1.27 at design corrected weight flow and with multiple flap bypass doors at 0°, 5°, and 10° flap angle are presented in figure 10. All three evaluation parameters (i.e., total pressure recovery, steady-state distortion, and dynamic distortion) deteriorated considerably with angle of attack. The highest pressure recovery at 10° angle of attack was 0.942 with the 5° flaps and the lowest was 0.896 with the 10° flaps. The closed bypass door configuration yields a recovery of 0.926 between the other two configurations. This varying performance trend indicates that at angle of attack a different scheduling of bypass door flap angle may be required. The increase in the steady-state distortion with angle of attack was roughly 0.05 for both the 0° and 5° bypass door flap configuration. The increase in steady-state distortion for the 10° bypass flap was 0.11. The spread in dynamic distortion is from 0.005 at 0° angle of attack to roughly 0.017 at 10° angle of attack depending on bypass door flap angle.

Pressure recovery. - The performance at the design corrected engine weight flow of the 60-40 T inlet is presented in figure 11 as a function of bypass mass flow ratio ($\alpha = 0$) for the series of Mach numbers tested. Both multiple and single flap data are presented. Except for the 10° bypass door flap angle all pressure recoveries fell in a band from 0.975 to 0.990 for all the transonic Mach numbers tested and for both the single and multiple flap bypass door configurations. When the flaps were set at 10° the total pressure recovery varied from 0.94 at $M_0 = 1.1$ to 0.98 at $M_0 = 0.80$.

Distortion. - For all the Mach numbers tested except 0.8 and for all configurations tested the steady-state distortion always lies within the 0.05 to 0.07 range at zero bypass mass flow spillage, and all increased monotonically to 0.15 to 0.17 at a roughly 0.12 bypass mass flow. Except for two single flap high bypass mass flow conditions the dynamic distortion was always less than 0.01.

To present a more detailed picture of how the bypass door configuration affects the steady-state distortion, four contour plots at the design corrected weight flow are presented in figure 12. The duct struts that are indicated in the figure start 5.546 compressor face duct heights upstream and extend 0.230 duct height downstream of the compressor face measuring station. At a free stream Mach number of 1.27 (fig. 12) there is a gradual thickening of the centerbody boundary layer between the bypass doors as the multiple flaps opened from their closed position (fig. 12(a)) to 5° (fig. 12(b)) and then to 10° flap angle (fig. 12(c)). The greater the bypass flow the greater the distortion. At large bypass flows the poorest recovery is occurring at the circumferential location midway between bypass doors. To further depict this point the radial total pressure recovery obtained from a rake located midway between two adjacent bypass openings is included on each contour map. The distortions are more severe at a free stream Mach number of 1.27 than at 0.8 as demonstrated by comparing figure 12(b) with 12(d).

The dynamic distortion data at the design corrected weight flow (fig. 13) and at a flow larger than the design corrected weight flow (fig. 14) is compared with total pressure recovery for free stream Mach numbers of 0.8 and 1.27. The dynamic data and total pressure recovery were taken during different runs so that compressor face mass flow, bypass mass flow, and free stream Mach number may be somewhat different between comparable data. Nevertheless, a generalization can be made about dynamic distortion: The largest dynamic distortion occurs where there is a steep gradient in total pressure recovery. This characteristic is exhibited for all free stream Mach numbers tested. Whenever the gradient of the total pressure is small, such as is presented in figure 13(c), the rms total pressures obtained are also small. In addition, data from various bypass door configurations are also presented in the figures. It can be seen by comparing figures 13(a), (b), and (c) that the flap angle setting of the multiple flap doors does not affect the local magnitude of the dynamic pressures. The sensitivity of the localized dynamic distortion to the internal flow conditions is demonstrated in figure 14(a) where the compressor face mass flow ratio has been increased slightly above that measured at the design point (fig. 13(c)).

To further examine the dynamic distortion, power spectral densities (PSD) were taken at a few supercritical mass flows at each of the five transducers used in the model. These PSD's along with tunnel wall static transducer data taken near the inlet station are presented in figure 15(a) for a configuration with 10^{o} multiple flap bypass doors and tested at Mach 1.27. The corresponding rms and averaged total pressures are presented in figure 14(a). Generally, the wind tunnel signatures at 740, 800, and 860 hertz appear on the recording of all but one transducer. The peak magnitude in the PSD of the signatures for the compressor face total pressures all fall between 10^{3} and 10^{4} (newtons per square meter)^{2} per hertz, while the peak for the tunnel static is roughly a tenth of this value. The PSD's of the pressure taken in the high shear layer do not exhibit any trace of the tunnel signature, because the signature is swamped by the background noise occurring at this location in the diffuser flow. The PSD's of the tunnel signature are small, since they are only observable when the rms's of the dynamic pressures are less than 0.015 of the local total pressure. The tunnel signatures that occur at 1925 and 2375 hertz are not detected at the compressor face station. These disturbances are primarily due to "tunnel-bleed-hole" interaction and are noise generated at the tunnel wall (ref. 4). The disturbance near 800 hertz originates from the tunnel compressor since the compressor speed is controlled from 840 to 880 rpm and there are 60 blades in the last stage of the compressor.

At a free stream Mach number of 0.8, which is presented in figure 15(b), the same general observations can be made. There is a new tunnel signature at 1720 which also appears in the diffuser of the inlet. This latter signal is close to the first harmonic of the grouping that lies near 800 hertz.

Inlet Drag

The variation of total drag coefficient with bypass flow at designed corrected weight flow is shown in figure 16. It can be seen that at the high Mach numbers it is advantageous to spill air through the bypass doors rather than over the cowl. Conversely, at low Mach numbers it is advantageous to spill all the air over the cowl. As the bypass mass flow ratio varies from 0 to 0.12 the greatest variation in total drag coefficient occurs at Mach 0.9 and 1.0. Consequently, the drag at Mach 0.9 and 1.0 is more sensitive to bypass door setting than at 0.8, 1.1, 1.2, and 1.27.

The total drag coefficient as a function of the bypass mass flow at different compressor face mass flows is presented in figure 17. At all zero bypass mass flow conditions the larger the engine mass flow the smaller the total inlet drag. The same general conclusions can be made when the bypass flaps are set at 5° with the exception at a free stream Mach number of $M_0 = 0.8$. At a flap angle of 10° there are some conditions where intermediate and low values of engine mass flow ratio (i.e., 0.550 and 0.425) will yield roughly the same total inlet drag. The smallest sonic drag rise occurs when the engine mass flow is largest. At all Mach numbers except Mach 1.27 the inlet drag may increase or decrease with the bypass mass flow depending on whether the engine mass flow is large or small.

The inlet total drag at constant inlet mass flow is more sensitive to the bypass door flap design than is indicated on the summary plot (fig. 9(b)), which applies only for constant engine flow. In figure 18 the inlet total drag coefficient is plotted as a function of the bypass mass flow ratio for two inlet mass flows, single and multiple flap doors, and various Mach numbers. There is no combination of mass flow and Mach number in which the single flap doors are better than the multiple flap doors. In every case tested the drag increment is a monotonic function of bypass mass flow ratio. At an inlet mass flow ratio of roughly 0.58 and Mach numbers of 1.1, 1.0, and 0.9, the difference in total inlet drag between the single and multiple flap bypass door configuration is generally smaller than the difference that exists at larger engine mass flow, that is, roughly 0.67. All the experimental data of total drag coefficients over the range of mass flows tested are presented for reference only in figures 23, 24, and 25.

Cowl drags. - Cowl drags were obtained by area weighting the static pressures over the cowl frontal area. These cowl drags are presented in figure 19(a) as a function of inlet capture mass flow. It depends on the test conditions whether or not the inlet dumps additional mass flow through the bypass doors as the total inlet mass flow ratio is varied. There are sections of the curve which are actually an overlap of two different curves, one obtained from high bypass spillage and the other from a lower bypass spillage but with a little higher engine flow. For ease of reading values from the curves, the zero of each curve in figure 19(a) is displaced by 0.05 unit. The cowl drags and their respective

first derivatives as a function of inlet mass flow are both monotonic for each free stream Mach number tested except 0.8. At an inlet mass flow ratio of 0.65 the cowl drag coefficients are -0.026, -0.028, -0.030, -0.075, -0.082, and -0.085 at free stream Mach numbers of 1.27, 1.20, 1.1, 1.0, 0.9, and 0.8, respectively. Consequently, for a given spillage mass flow ratio of 0.35 over the lip there is a drag rise of 0.06 from Mach 0.8 to Mach 1.27. At an inlet mass flow ratio of 0.425 the cowl drag coefficients are -0.078, -0.100, -0.127, -0.193, -0.196, and -0.178 at free stream Mach numbers of 1.27, 1.2, 1.1, 1.0, 0.9, and 0.8, respectively. The drag rise from Mach 0.9 to Mach 1.27 is 0.12.

Additive drag. - The additive drag of the transonic 60-40 T inlet is presented in figure 19(b) as a function of inlet mass flow for the six Mach numbers tested. The maximum theoretical mass flow ratio for supersonic spillage at $M_0 = 1.27$ is 0.775 (ref. 5), which is 0.02 greater than what was experimentally obtained. The zeros of the drag coordinate are shifted 0.05 unit for each free stream Mach number in a similar manner as with the cowl drag curves of figure 19(a). The additive drag coefficient is a linear function of inlet mass flow for free stream Mach numbers 1.27, 1.2, 1.1, and 1.0. Because the slope of the additive drag coefficient as a function of the inlet mass flow ratio curves are always greater than the slope of the cowl drag coefficients, it is always best to decrease additive drag when considering trading off cowl suction drag with additive drag except when $m_1/m_0 > 0.6$ for Mach 0.9 and 0.8. There may be an exception to this generalization at Mach 0.8 for the middle to larger inlet mass flows. If the anomaly of this drag curve is caused by terminal shocks resting on the cowl or centerbody surfaces, any conclusions made may not be applicable at a different Reynolds number, since body terminal shocks can be affected by a change in Reynolds number.

The sum of the cowl and additive drag is presented in figure 19(c). At Mach 0.9 and 0.8 the additive drag is totally recovered by a sharp edge cowl down to mass flows of 0.65 and 0.62, respectively. At greater Mach numbers the additive drag is not entirely recovered.

The important measurements used to determine the cowl and additive drag are wall statics on both the external centerbody and cowl surfaces. These wall statics are plotted in figure 20 for free stream Mach numbers 1.27, 1.0, and 0.8 at design corrected mass flow and when the multiple flap angles were set at 0°, 5°, and 10°. At Mach 1.27 with closed bypass doors the pressures on the centerbody surface increase rapidly to pressure values above the sonic value. This sonic value is indicated in figure 20 by an arrow pointing to the sonic pressure ratio. Any pressure ratios that lie above this mark are pressures for subsonic flow, and any pressure ratios below the mark are pressures for supersonic flow. The subsonic values at Mach 1.27 (fig. 20(a)) indicate that the terminal shock in the internal duct flow is setting close to the cowl face station of the inlet. As the bypass doors are opened to 5° and 10° the terminal shock can be seen to move back towards the cowl face station.

The external cowl pressures presented in figure 20(a) at Mach 1.27 indicate larger cowl suction (pressures less than free stream static) at the lip and at the second break in cowl contour. The high cowl pressure between these two low pressure regions indicates partial recovery of the cowl pressure to the value expected on an 8^{o} wedge with no subsonic spillage. Experimentally there is subsonic spillage since the theoretical supersonic spillage capture mass flow ratio at Mach 1.27 is 0.775 while the experimental value is 0.755. Because the magnitudes of the difference of these two mass flow ratios, the cowl lip bow shock must be close to the leading edge of the cowl, and, consequently, the local flow angle at the cowl lip is very close to the flow angle for supersonic spillage. The leading edge suction force effect, consequently, will be small and localized. As more air is spilled over the cowl, as with the 5^{o} flap angle or the no bypass configuration, the local flow angle at the cowl lip increases and the suction forces extent is larger, as can be seen in figure 20(a). Although there is a reduction in cowl drag, there is a concomitant increase in additive drag, the net effect being an increase in total drag. Consequently, for this Mach number the additive drag is not entirely recovered by the cowl suction forces. As less air is spilled over the cowl there is less favorable cowl suction, as demonstrated by the higher cowl pressures. The cowl suction force is even larger at Mach 1.0 than at Mach 1.27. At Mach 0.8 (fig. 20(c)) there is less lip suction force at the high lip spillage condition than at the higher subsonic Mach numbers tested.

The installation effect of mounting an inlet under a wing was investigated by testing the transonic 60-40 T inlet under a flat plate at a separation distance of roughly 0.13 cowl diameters. This distance was measured from the flat plate to the aft cylindrical portion of the inlet (0.21 cowl diam from wing to cowl lip). Total inlet drag and cowl drag coefficients at conditions with and without the wing simulator are compared in figures 21(a-1) and 21(b-1) as a function of free stream Mach number. At each bypass flap angle there exists a sizable transonic drag rise both with and without wing. Because of the assumed inlet engine flow matching, there is different mass flow spillage at practically each plotted point. Without a wing, the conventional drag rise is followed by a constant or decreasing drag with increasing Mach number by the time Mach 1.20 is reached. However, the drag data under a wing had not leveled out at the highest Mach number tested. If the drag coefficient without a wing is subtracted from the drag coefficient with a wing, an installation drag is obtained which is plotted in figure 21(b-2). There is no installation effect on total inlet drag until Mach 1.1 is reached. From Mach 1.1 up to and including 1.27, the largest Mach number tested, the drag increment increased almost linearly. The increment at Mach 1.27 is 0.100. Comparing the installation increment with the isolated total drag, figure 21(a-1), a drag increase of about 50 to 60 percent is observed with the presence of a wing.

The installation of a wing over a nacelle will change the external static pressures in the vicinity of the inlet entrance. A comparison of static pressures on the simulated

wing and nacelle for isolated and installed conditions is presented in figure 22 for a bypass multiple flap angle of 5^{o}. The differences in mass flow ratio of the inlet between the wing and no wing runs were small and are listed in the figure. The static pressure measured at Mach 1.27 is presented in figure 22. There are annotations in the figure to indicate the pressure that would result from a 10^{o} and 15.5^{o} cone angle and from a normal shock. With the installation of a wing the cone surface pressure is equivalent to that of a 15.5^{o} cone which may result from a flow separation on the plate and/or one on the centerbody that extends upstream to the centerbody tip. Although the bulk of the centerbody statics are taken along a circumferential angle of 90^{o}, at 0.5 cowl lip diameter back from the centerbody tip there are four statics, each 90^{o} from each other. The pressures measured by these four static tubes all agree to within the size of the symbol to indicate a symmetry in pressure measurement even though there is no asymuthal symmetry with respect to the installation configuration. The centerbody statics gradually increase to the normal shock value as we proceed downstream to the cowl lip. The presence of the wing increases the local drag forces near the lip by increasing the cowl pressures. Away from the cowl lip station downstream of the first break in the cowl contour the flow accelerates in the passage between the wing and nacelle; this is indicated by the reduced values of pressure measured in this region. At Mach 1.2 (fig. 22(b)) the same general conclusion can be made as was made with the data taken at Mach 1.27.

With a free stream Mach number of 1.1 the entire flow pattern around the centerbody tip with the isolated nacelle does not seem to follow the normal shock cone relations. With the installation configuration there appears to be a detached shock setting on the cone tip. At Mach 1.0 (fig. 22(d)) and 0.9 (fig. 22(e)) there is no installation effect except perhaps near the leading edge of the cowl lip.

In addition to the cone static pressures, total rake pressures were measured on a boundary layer rake mounted on the wing roughly 0.16 cowl diameter downstream from the spike tip and off to the side 0.755 cowl diameter. These rake data are presented in figure 22 at each of the Mach numbers tested. The boundary layer thickness is always smaller than the cowl lip wing separation distance except at Mach 0.8 where it is approximately equal to the installation separation distance.

The data shown in figure 22 indicate that the increases in cowl drag and total inlet drag due to the installation effect originate from cone shocks reflecting off the wing onto the model and/or compression waves impinging on the model from a possible thickened boundary layer. These increased pressures will then result in larger additive drags and large cowl drags. The basic total drag data as a function of engine mass flow at various flap angle conditions and with and without boundary plate are presented in figure 25.

SUMMARY OF RESULTS

The transonic performance, including both pressure and drag data, of an inlet designed for Mach 2.5 with a design contraction split of 60-40 was tested over the Mach 0.8 to 1.27 range. The Reynolds number of the axisymmetric 25.4-centimeter model was roughly 3.7×10^6. The inlet was basically designed by scaling down the dimensions of configurations that had been tested previously at their design speeds. Excessive internal contraction that would be present at below design speeds is eliminated by collapsing various surfaces and parts and by translating the centerbody of the scaled-down inlet. The measurement of the total drag of the configuration with the use of a load cell enabled the drag to be broken down into additive, cowl, and friction drag. The following is a summary of results from the test:

1. At Mach 0.8 the inlet drag decreases when the bypass doors of the inlet are closed and the excess air flow is spilled over the cowl.

2. At Mach 1.27 the inlet drag is lowest when the bypass doors are partially open in order to spill excess ingested air.

3. Even on the sharp edge of the cowl lip, suction force played an important role. The cowl lip suction force was responsible for the decrease in total drag at subsonic speeds as more air is spilled over the cowl.

4. For small flap angles there is no drag difference between multiple and single flap bypass doors; at larger flap angles the single flap doors gave a larger drag.

5. The presence of the wing results in a sizable increase of the inlet drag at high transonic speeds.

Lewis Research Center,
National Aeronautics and Space Administration,
Cleveland, Ohio, January 4, 1974,
501-24.

APPENDIX A

SYMBOLS

A	cross-sectional area, cm^2
A_c	capture area, cm^2
C_{DA}	additive drag coefficient, $drag/q_0A_c$
C_{DC}	cowl drag coefficient, $drag/q_0A_c$
C_{DT}	total inlet drag coefficient, $drag/q_0A_c$
D_c	diameter of cowl lip, 21.87 cm (8.612 in.)
F_{lc}	force measured on load cell, N
h	distance from centerbody surface, cm
I	impulse function, $pA + p\gamma AM^2$, N
M	Mach number
m	mass flow, kg/sec
P	total pressure, N/m^2
P_{max}	maximum total pressure at compressor face station, N/m^2
P_{min}	minimum total pressure at compressor face station, N/m^2
P_{rms}	root mean square of instantaneous pressure, N/m^2
PSD	power spectral density, $(N/m^2)^2/Hz$
$\bar{P}_2$	average total pressure at compressor face station, N/m^2
ΔP	$P_{max} - P_{min}$, N/m^2
p	static pressure, N/m^2
q	dynamic pressure, $\gamma pM^2/2$, N/m^2
R	radius, cm
ΔR	local duct height, cm
$w\sqrt{\theta}/\delta A$	corrected weight flow, $kg/sec/m^2$
X	axial distance from spike tip, cm
Y	perpendicular distance from wing simulator surface, cm
Z	axial distance from cowl tip, cm
α	angle of attack, deg

Subscripts:

BL boundary layer

bp bypass

0 free stream station

1 cowl lip station

2 compressor face station

3 mass flow measuring station

APPENDIX B

DRAG CALCULATIONS

The sketch in this appendix represents two different spillage configurations. One configuration uses the multiple flap bypass door where the inlet captures an $A_{0,bp}$ free stream tube of air. Since the engine is only to accept an $A_{0,3}$ free stream tube, the difference $(A_{0,bp} - A_{0,3})$ is dumped out the bypass doors. The dots in the sketch annotate the dump air stream tube. The other spillage configuration uses a closed bypass. Here the capture free stream tube is represented by $A_{0,3}$. The dashed line traces this stream tube through the inlet.

This sketch depicts a decrease in additive drag, because of a decrease in frontal area of the free stream capture tube, whenever the bypass doors are open. There will be a penalty, however, associated with the bypass dumping of the air which is related to the nozzle efficiency of the doors.

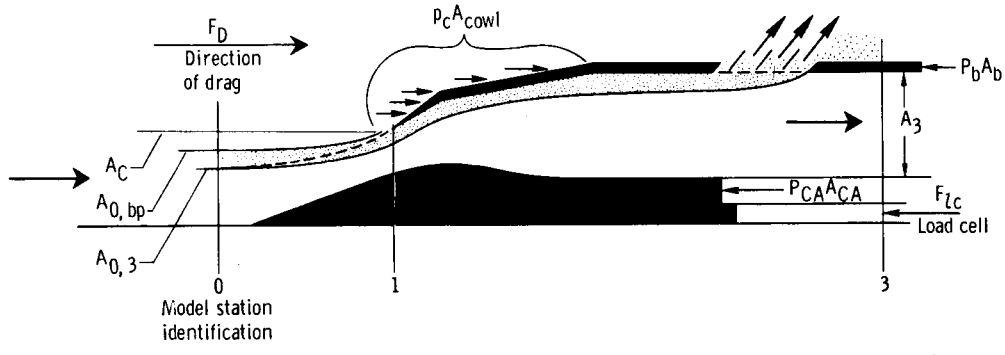

The various drag terms used in the report were calculated by using the following expressions:

$$F_A = (I_1 - I_0) + \sum p_{cone} \Delta A_{cone} - p_0(A_c - A_{0,bp})$$

$$F_C = \sum p_c \Delta A_{cowl}$$

$$F_F = C_f S_f q_0$$

where

$$C_f = f(M_0) \quad \text{(ref. 6)}$$

and S_f is the external wetted flow area.

$$F_T = F_{lc} + I_3 - I_0 + p_b A_b + p_{CA} A_{CA} - p_0 (A_b + A_{CA} + A_3 - A_{0,bp})$$

where

$$I_0 = 2q_0 A_{0,bp} + p_0 A_{0,bp}$$

$$I_1 = p_1 (A_c - A_{cone}) + \gamma p_1 M_1^2 (A_c - A_{cone})$$

$$I_3 = p_3 A_3 + \gamma M_3^2 p_3 A_3$$

$$A_{0,bp} = A_c \frac{m_1}{m_0}$$

and

F_A additive drag

F_C cowl drag

F_F friction drag

F_T total inlet drag

I impulse function

with the subscripts

CA cavity

cone cone

cowl cowl

b base

The actual drag coefficients are obtained by dividing the previously listed drags by $q_0 A_c$.

REFERENCES

1. Koenig, Robert W.: Inlet Sensitivity Study for a Supersonic Transport. NASA TN D-3881, 1967, pp. 20-21.

2. Neale, M. C.: and Armstrong, F. W.: Some Recent Research on Supersonic Intakes at NGTE. Aerodynamic Interference. Conf. Proc. 71-71, AGARD, Jan. 1971.

3. Wasserbauer, Joseph F.; and Choby, David A.: Mach 2.5 Performance of a Bicone Inlet with Internal Focused Compression and 40-Percent Internal Contraction. NASA TM X-2294, 1971.

4. Karabinus, Raymond J.; and Sanders, Bobby W.: Measurements of Fluctuating Pressures in 8- by 6-Foot Supersonic Wind Tunnel for Mach Number Range of 0.56 to 2.07. NASA TM X-2009, 1970.

5. Mascitti, Vincent R.: Charts of Additive Drag Coefficient and Mass-Flow Ratio for Inlets Utilizing Right Circular Cones at Zero Angle of Attack. NASA TN D-3434, 1966.

6. Smith, K. G.: Methods and Charts for Estimating Skin Friction Drag in Wind Tunnel Tests with Zero Heat Transfer. Rep. ARC-CP-824, Aeronautical Research Council, Great Britain, 1965.

TABLE I. - INLET COORDINATES

[60-40 T inlet lip station, 1.3852; centerbody translation, 0.2909.]

Centerbody		Cowl, internal		Cowl, internal	
X/D_c	R/D_c	Z/D_c	R/D_c	Z/D_c	R/D_c
0.0000	0.0000	0.0000	[a]0.5000	1.4644	0.5022
.2322	.0409	.0448	.5039	1.5030	.5051
1.4145	.2494	.1029	.5086	1.5631	.5098
1.4293	.2520	.1609	.5127	1.6191	.5135
1.4873	.2629	.2190	.5159	1.7353	.5174
1.5454	.2697	.2771	.5182	1.8514	.5195
1.6035	.2717	.3351	.5193	1.9675	.5207
1.6615	.2697	.3932	.5188	2.0466	.5214
1.7196	.2679	.4512	.5172	2.0836	.5217
1.7776	.2661	.5093	.5152	2.2175	.5225
1.8357	.2642	.5673	.5136	2.4497	.5208
1.8938	.2610	.6254	.5122	2.5658	.5179
1.9518	.2563	.6835	.5107	2.6820	.5153
2.0099	.2490	.7415	.5091	2.7400	.5142
2.0679	.2414	.7996	.5072	2.7981	.5135
2.1260	.2327	.8576	.5049	2.8045	.5134
2.1840	.2253	.9157	.5020	2.9206	.5134
2.2421	.2182	.9738	.4993		
2.3002	.2120	1.0318	.4971	Cowl, external	
2.3582	.2058	1.0899	.4957	Z/D_c	R/D_c
2.4163	.1998	1.1479	.4951		
2.4743	.1962	1.2060	.4949	0.000	[a]0.5023
2.5324	.1931	1.2641	.4951	.3140	.5464
2.5586	.1916	1.3221	.4962	1.4644	.5806
2.8495	.1916	1.3802	.4981		
4.1802	.2584	1.4382	.5008		

[a]Tip radius, 2.54×10^{-2} centimeter.

TABLE II. - STATIC PRESSURE TAP LOCATIONS FOR 60-40 T INLET

[Diameter of cowl lip, D_c = 21.87 cm.]

Centerbody[a] tap location, X/D_c	Cowl[b] tap location, Z/D_c
0.2861	0.01219
.4955	.06897
.6396	.1247
.7568	.1798
.8581	.2341
.9487	.2875
1.0314	.3420
1.1079	.4126
1.1794	.4828
1.2469	.6082
1.3108	.8018
1.3718	.9934
cowl station 1.3850	1.1831
	1.3710

[a]Measured from 90° side centerline.
[b]Zero degree top centerline.

TABLE III. - MASS FLOW RATIO CORRESPONDING TO DESIGN CORRECTED WEIGHTFLOW OF 60-40 T INLET

Mach number, M_0	Mass flow ratio, m_3/m_0		
	No bypass	5° bypass	10° bypass
1.27	0.651	0.651	0.633
1.20	.6455	.6455	.625
1.10	.642	.642	.618
1.00	.6415	.645	.628
.90	.647	.647	.6375
.80	.656	.659	.655

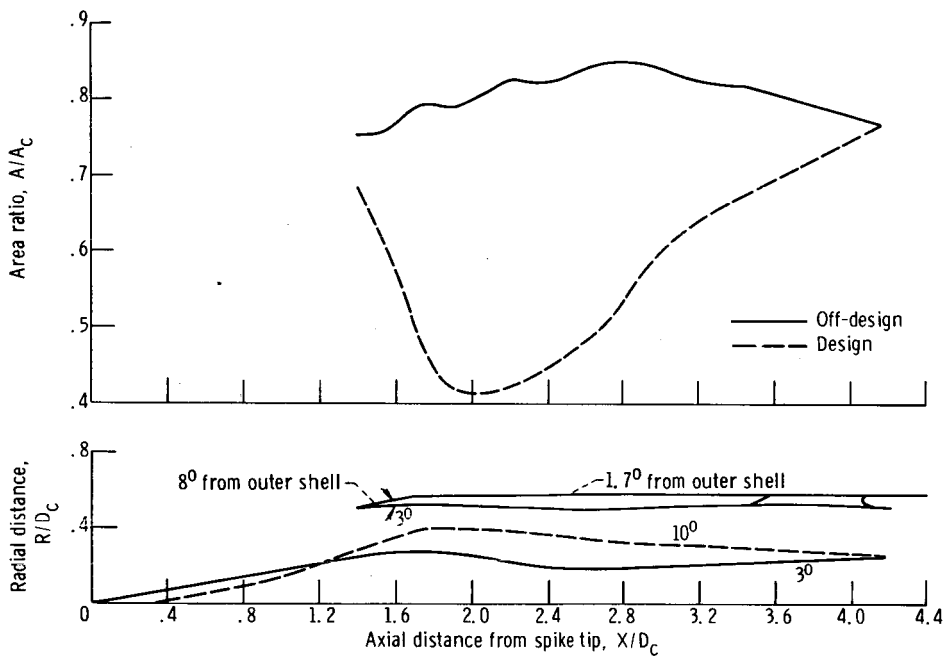

Figure 1. - Geometry of design and off-design configuration of 60-40 T inlet. Centerbody translated 0.2909 cowl diameter.

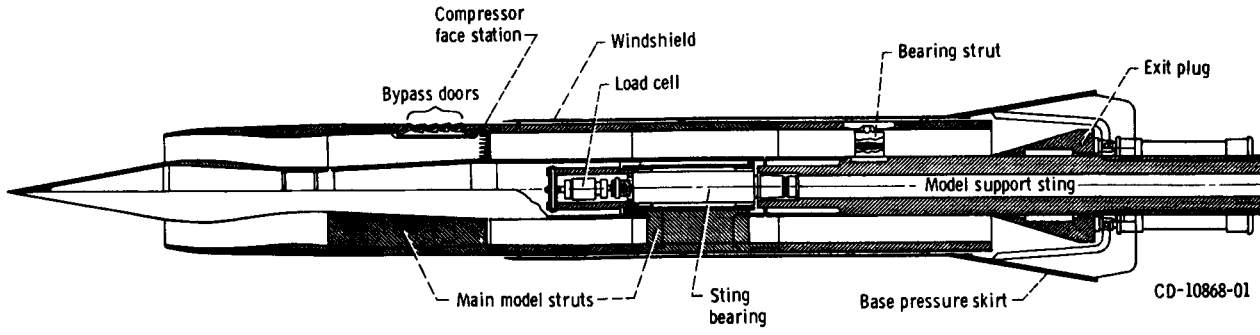

(a) Schematic showing flow passages.

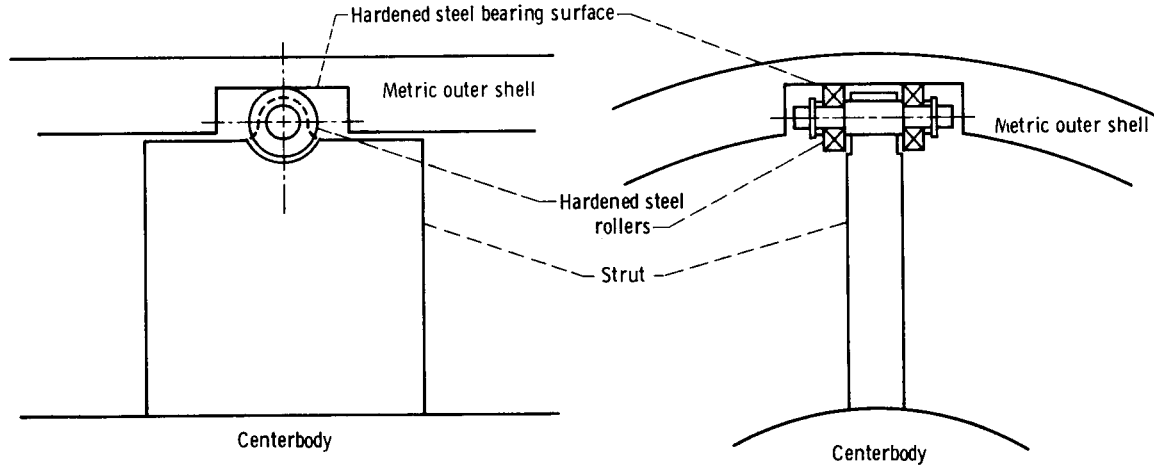

(b) Strut bearing; bearing shimed to allow 0.0127 to 0.0178 centimeter clearance with rollers.

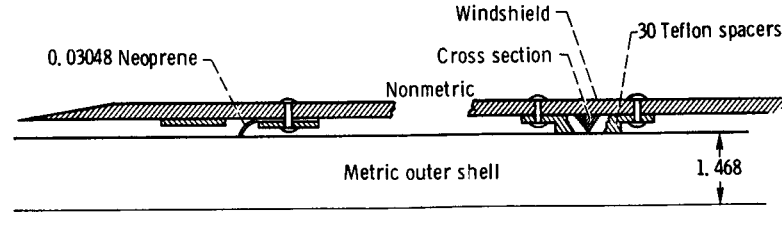

(c) Bearing surface between outer shell nonmetric (windshield) and 25.4-centimeter metric cylinder. All dimensions in centimeters.

Figure 2. - Model schematic.

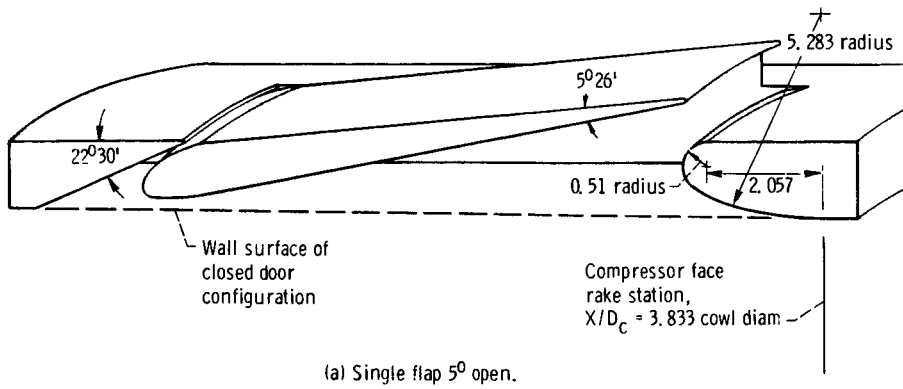

(a) Single flap 5° open.

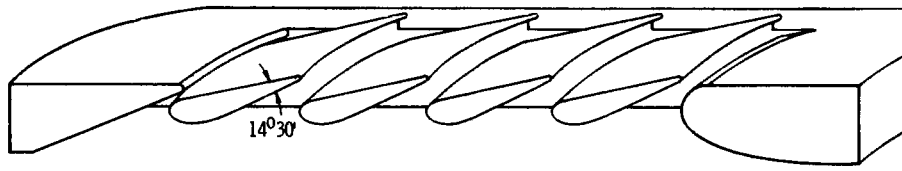

(b) Multiple flap 10° open.

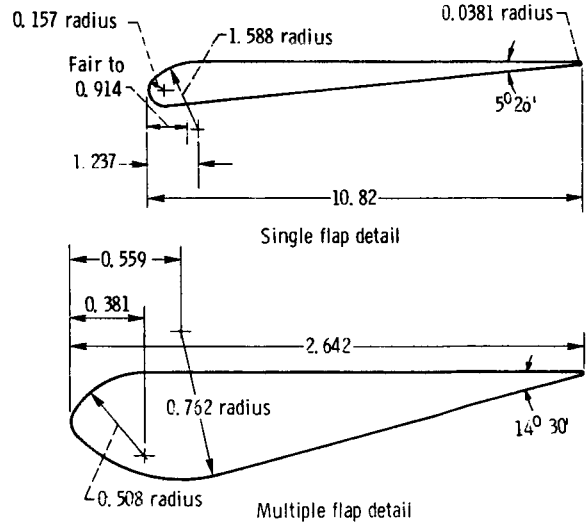

(c) Cross section detail of flaps. Door width, 6.558 centimeters.

Figure 3. - Detail of bypass door configuration. All dimensions in centimeters unless otherwise noted.

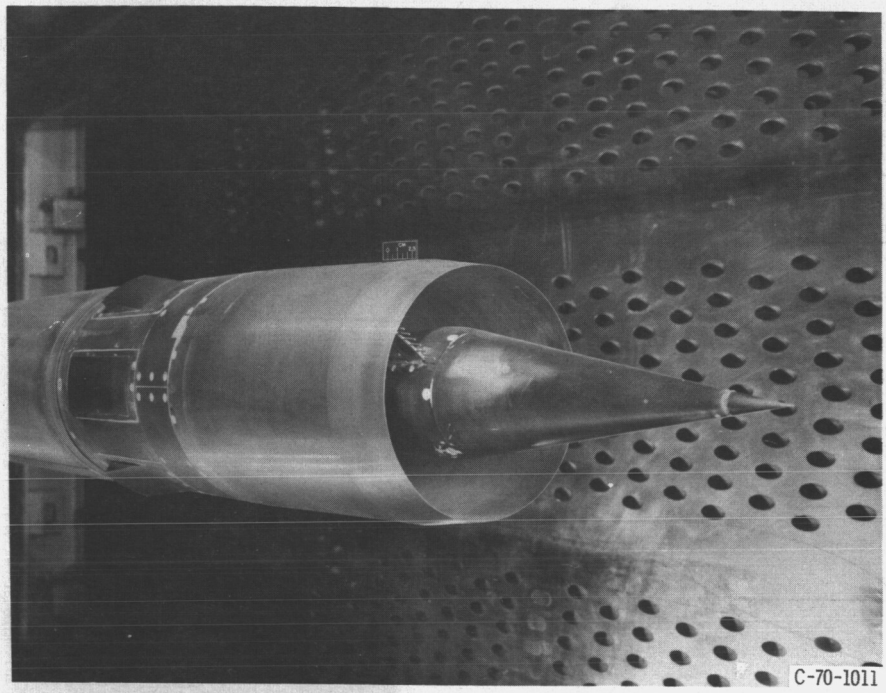

Figure 4. - 60-40 T inlet with 10^0 single flap bypass doors mounted in Lewis Research Center 8 by 6 Foot Supersonic Wind Tunnel.

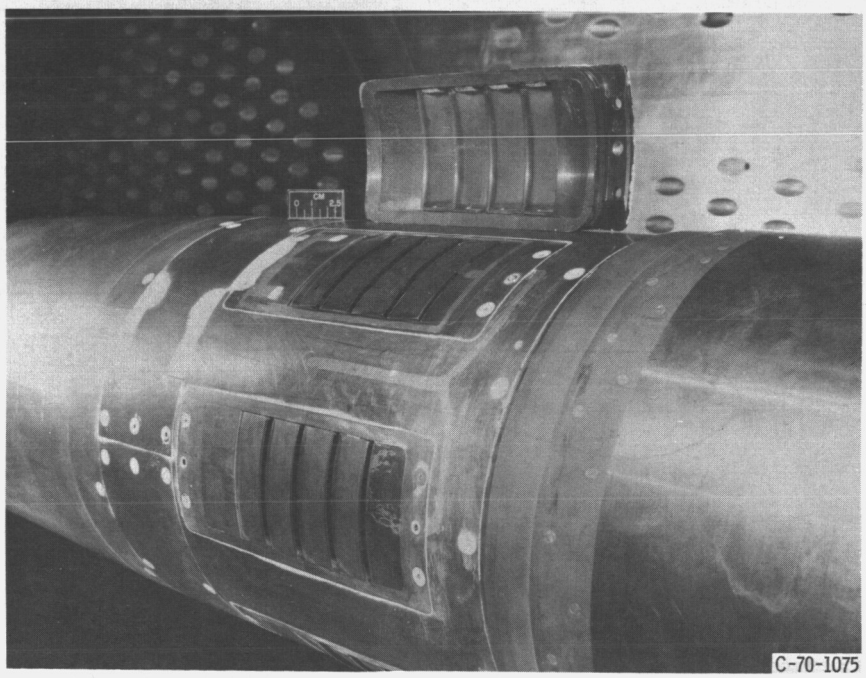

Figure 5. - 5^0 Multiple flap bypass doors looking upstream. On top of model is underside view of spare multiple flap door insert.

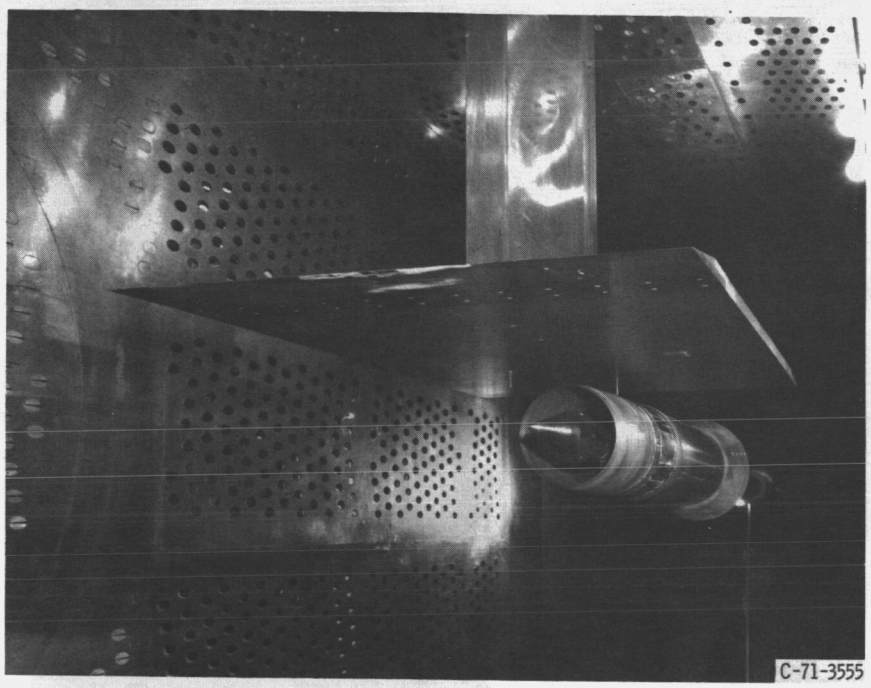

Figure 6. - 60-40 T inlet without bypass doors mounted under wing simulator in Lewis Research Center 8 x 6 Foot Supersonic Wind Tunnel.

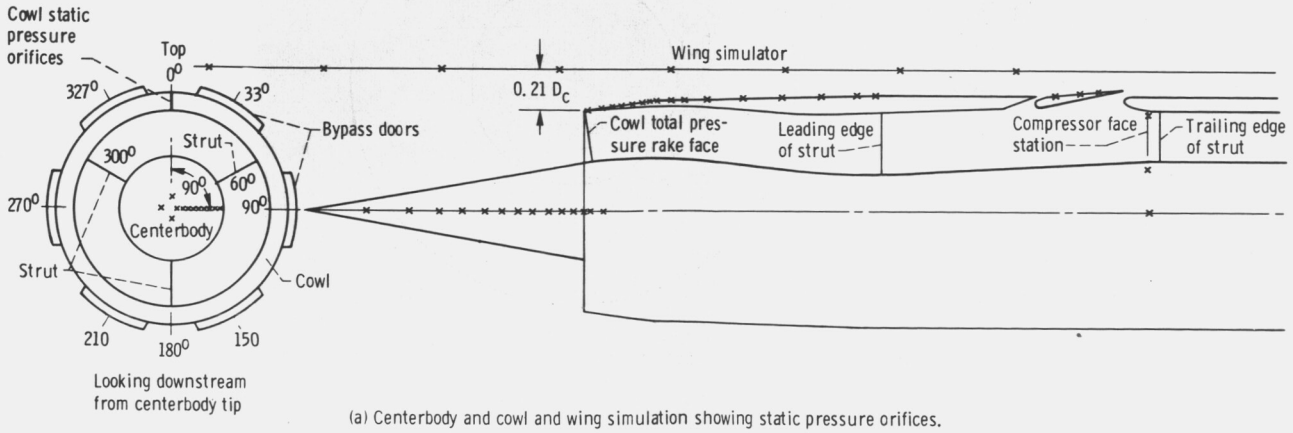

(a) Centerbody and cowl and wing simulation showing static pressure orifices.

Figure 7. - Model instrumentation.

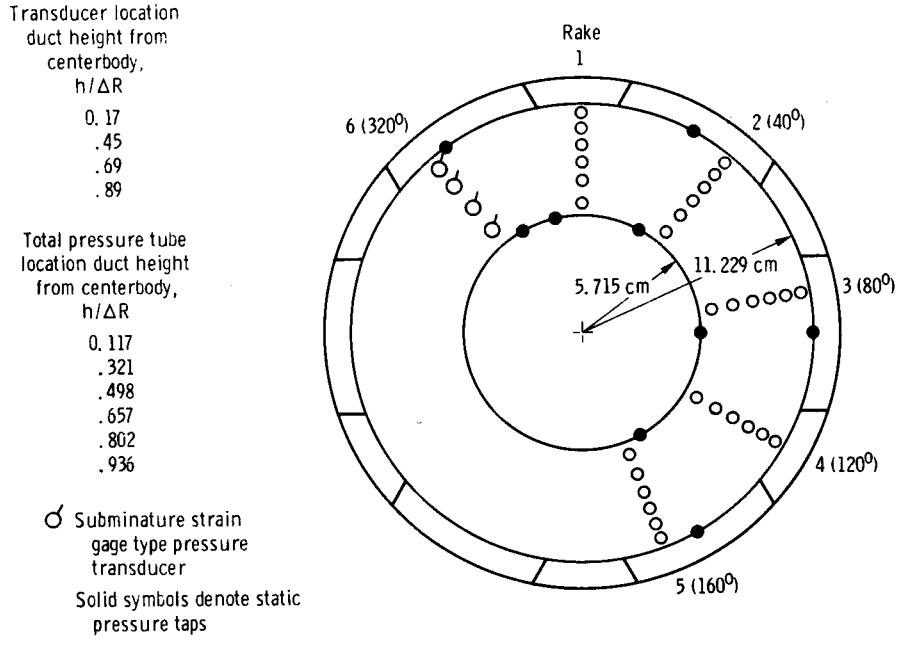

(b) Compressor face instrumentation. Model station, 3.833 cowl diameters. Looking downstream at compressor face rakes and statics.

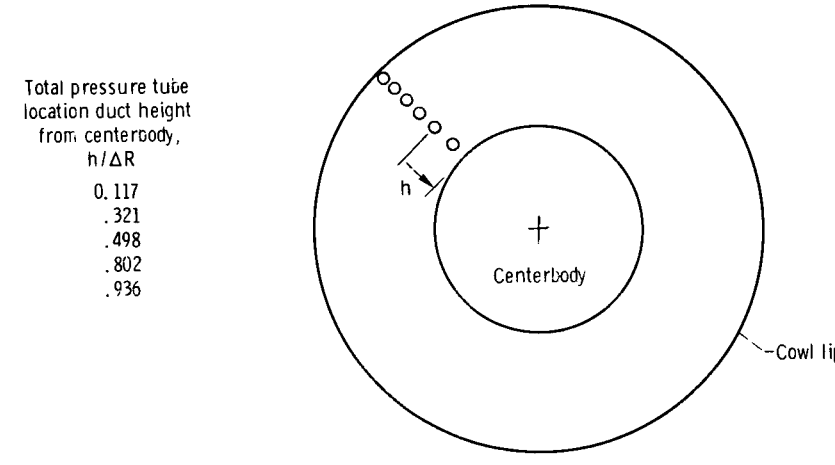

(c) Cowl face instrumentation. Looking downstream at cowl face rake.

Figure 7. - Concluded. Model instrumentation.

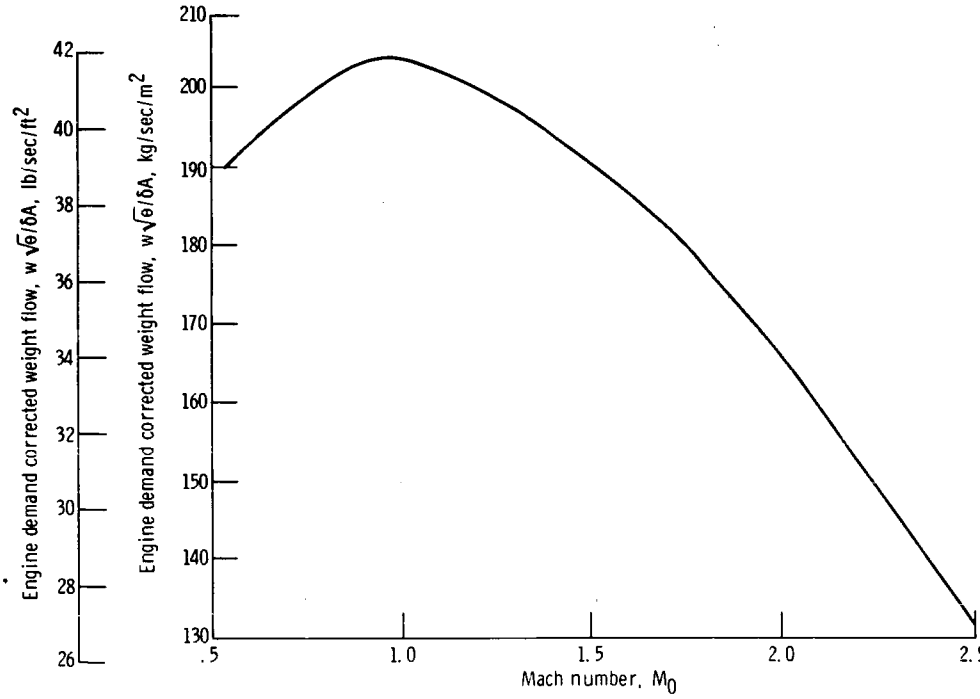

Figure 8. - Design corrected engine weight flow as function of Mach number.

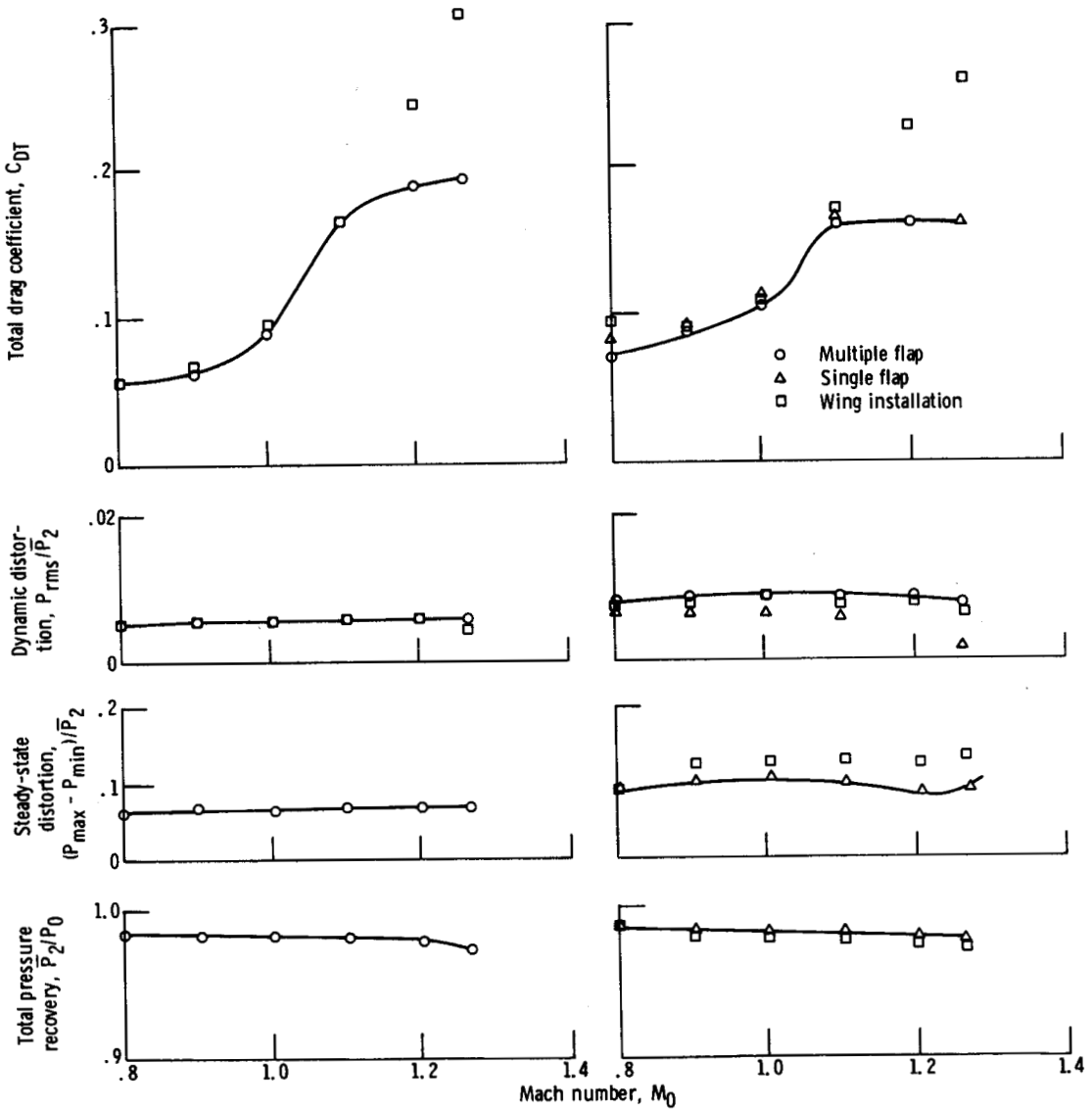

(a) Bypass doors closed.

(b) Bypass doors flap angle, 5^0.

Figure 9. - Summary performance of 60-40 T inlet at design corrected weight flow.

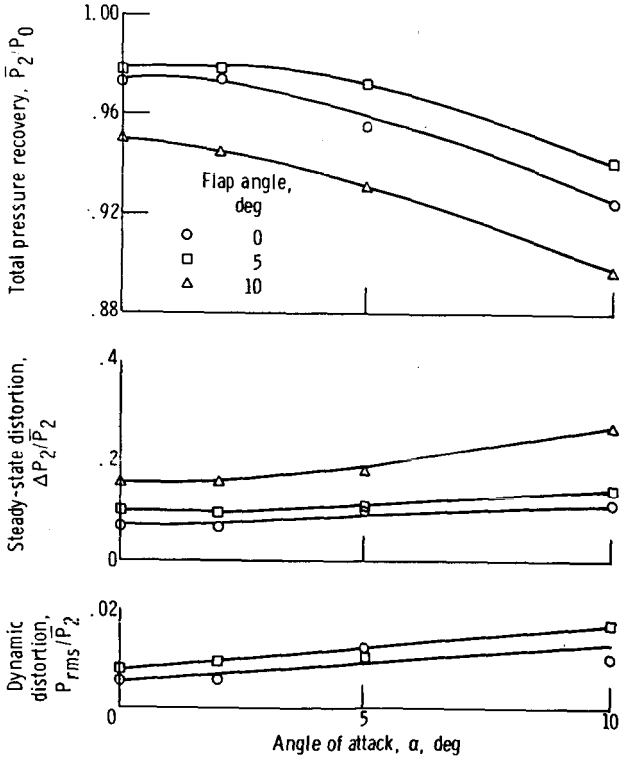

Figure 10. - 60-40 T inlet performance as function of angle of attack at Mach 1.27 and design corrected weight flow and with multiple flap bypass doors.

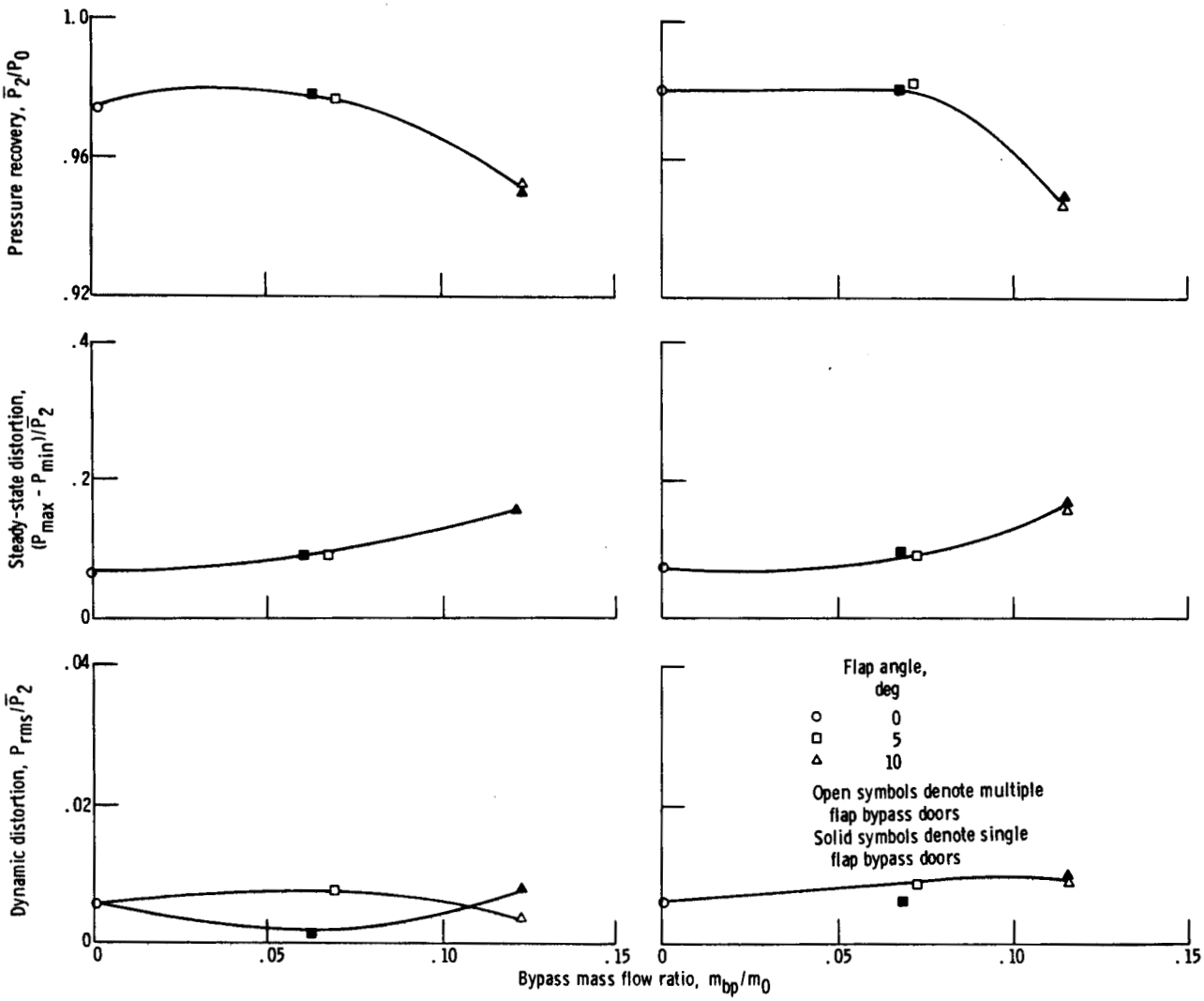

(a) Mach number, M_0 = 1.27.

(b) Mach number, M_0 = 1.2.

Figure 11. - Variation of performance of 60-40 T inlet with bypass mass flow ratio at design corrected weight flow.

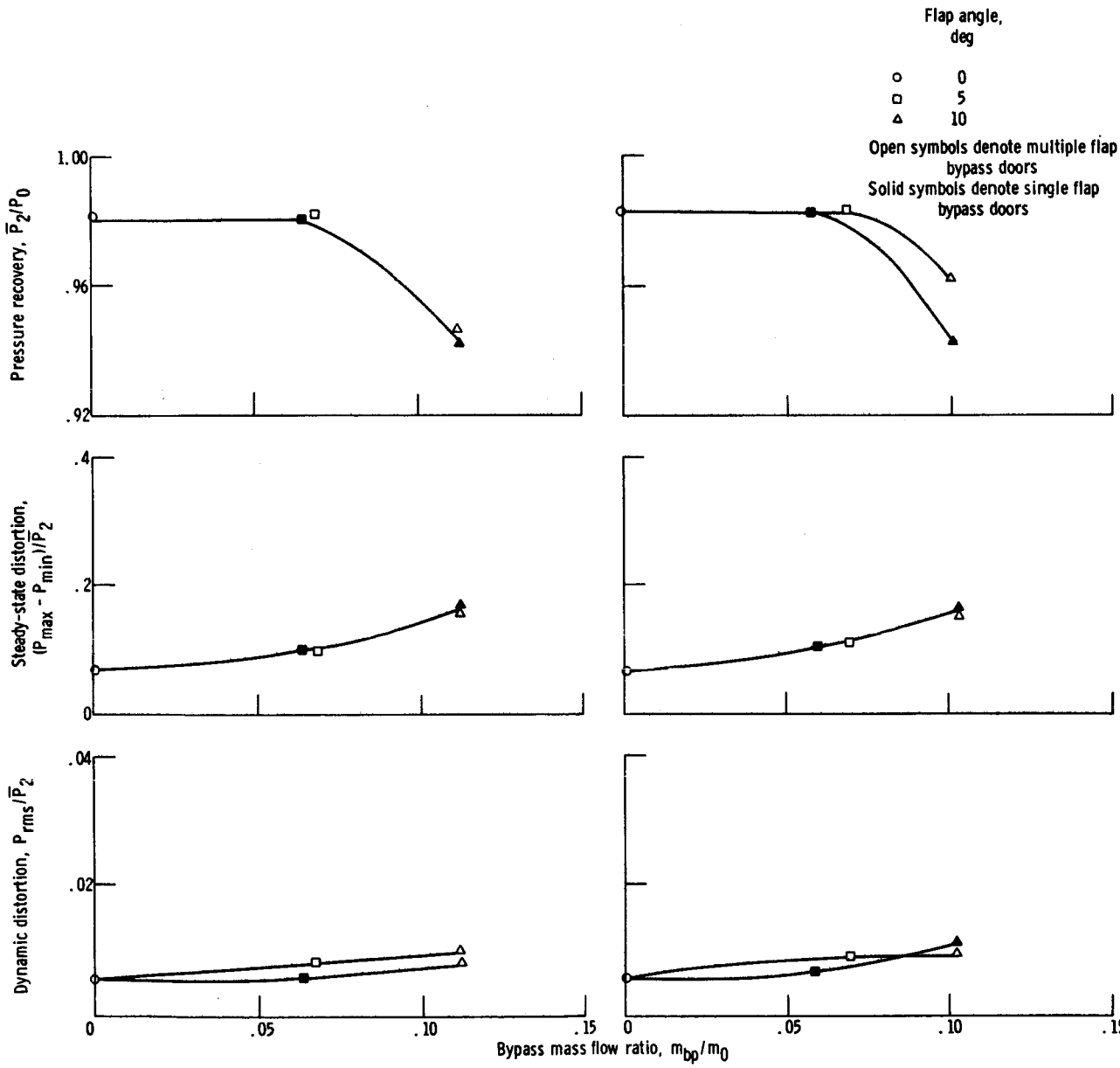

(c) Mach number, $M_0 = 1.1$.

(d) Mach number, $M_0 = 1.0$.

Figure 11. - Continued.

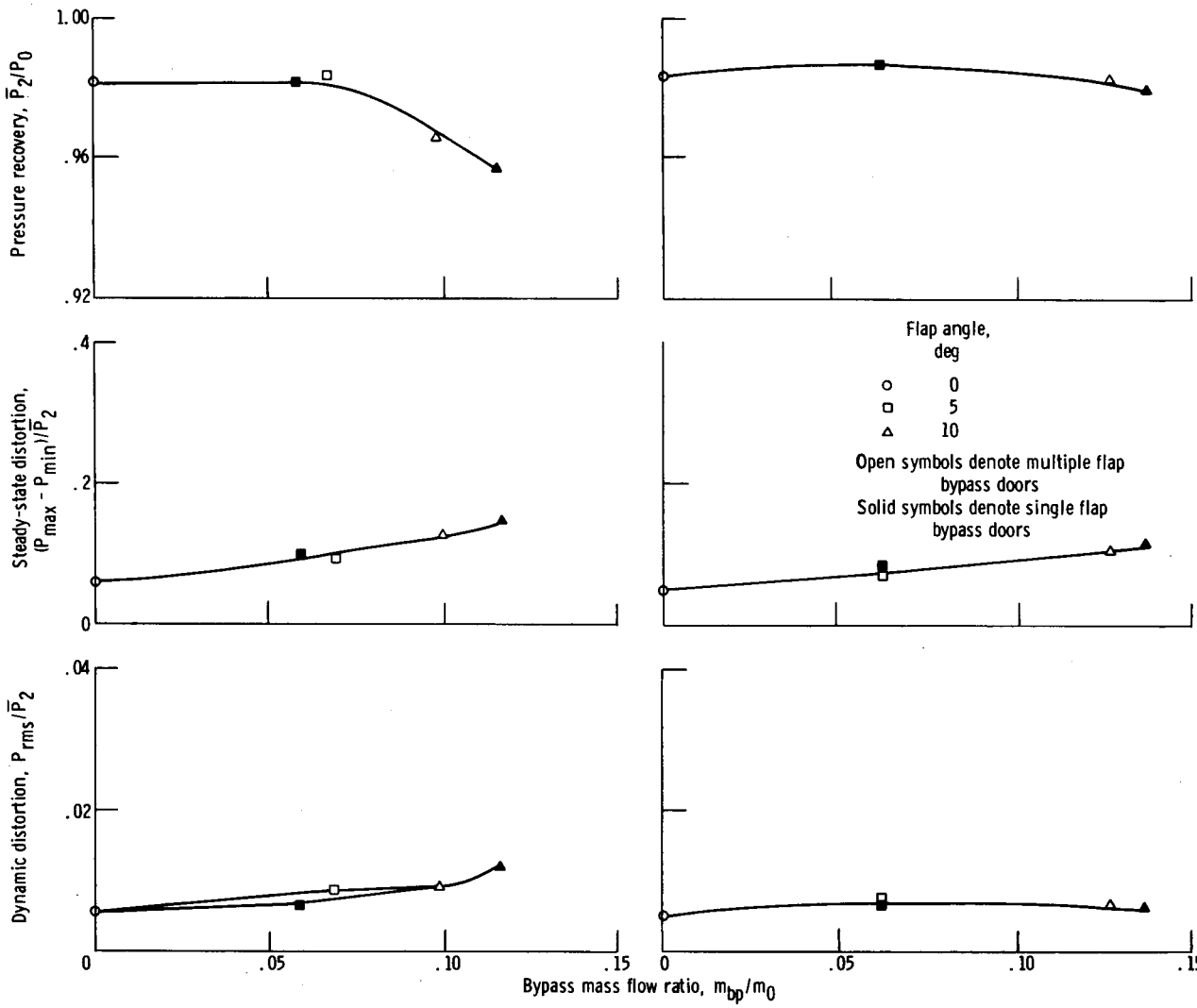

(e) Mach number, $M_0 = 0.9$.

(f) Mach number, $M_0 = 0.8$.

Figure 11. - Concluded.

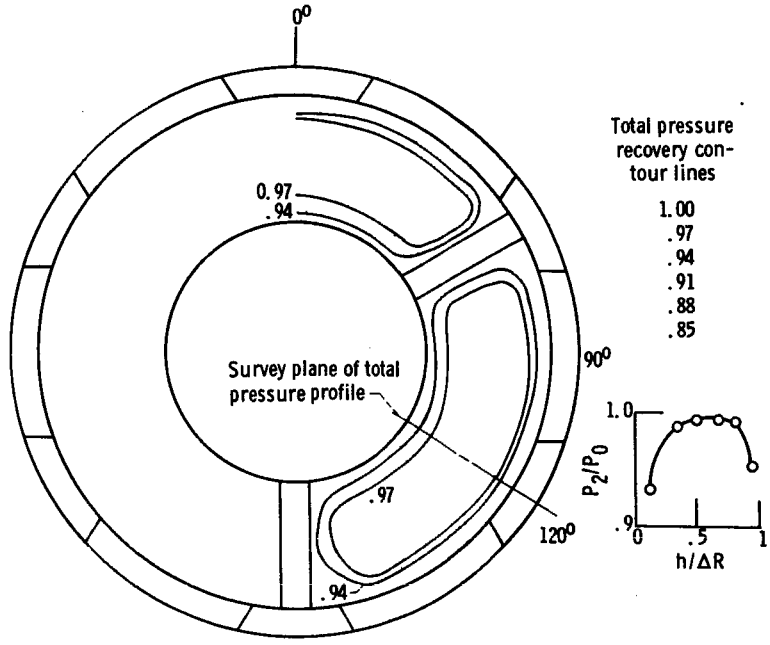

(a) Mach number, $M_0 = 1.27$; bypass doors closed. Bypass mass flow ratio, $m_{bp}/m_0 = 0$; average total pressure recovery, $\bar{P}_2/P_0 = 0.975$; mass flow ratio, $m_3/m_0 = 0.650$; pressure ratio, $(P_{max} - P_{min})/\bar{P}_2 = 0.069$.

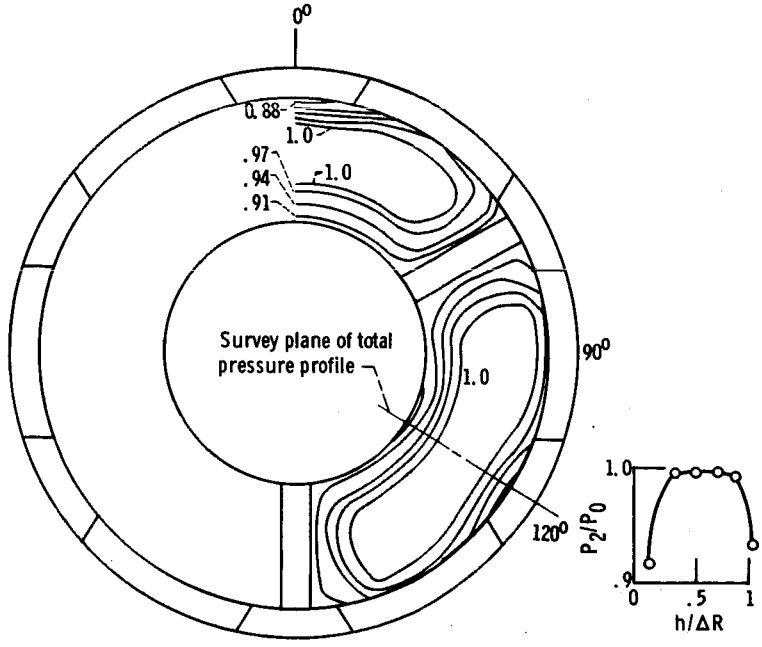

(b) Mach number, $M_0 = 1.27$; 5° multiple flap doors. Bypass mass flow ratio, $m_{bp}/m_0 = 0.069$; average total pressure recovery, $\bar{P}_2/P_0 = 0.978$; mass flow ratio, $m_3/m_0 = 0.652$; pressure ratio, $(P_{max} - P_{min})/\bar{P}_2 = 0.0945$.

Figure 12. - Total pressure recovery contours at compressor face station of 60-40 T inlet at design corrected weight flow. Looking downstream at compressor face rake station 3.832.

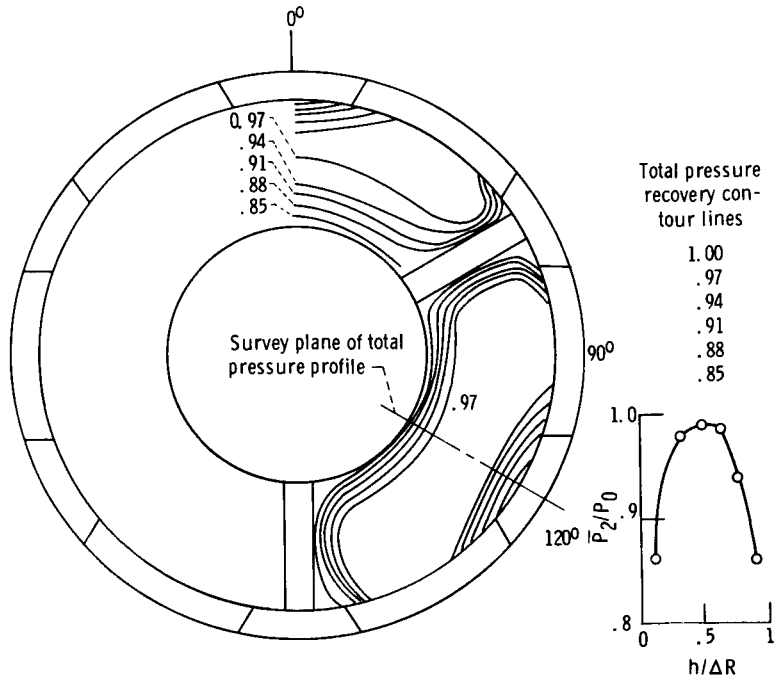

(c) Mach number, $M_0 = 1.27$; 10° multiple flap doors. Bypass mass flow ratio, $m_{bp}/m_0 = 0.122$; average total pressure recovery, $\bar{P}_2/P_0 = 0.951$; mass flow ratio, $m_3/m_0 = 0.833$; pressure ratio, $(P_{max} - P_{min})/\bar{P}_2 = 0.154$.

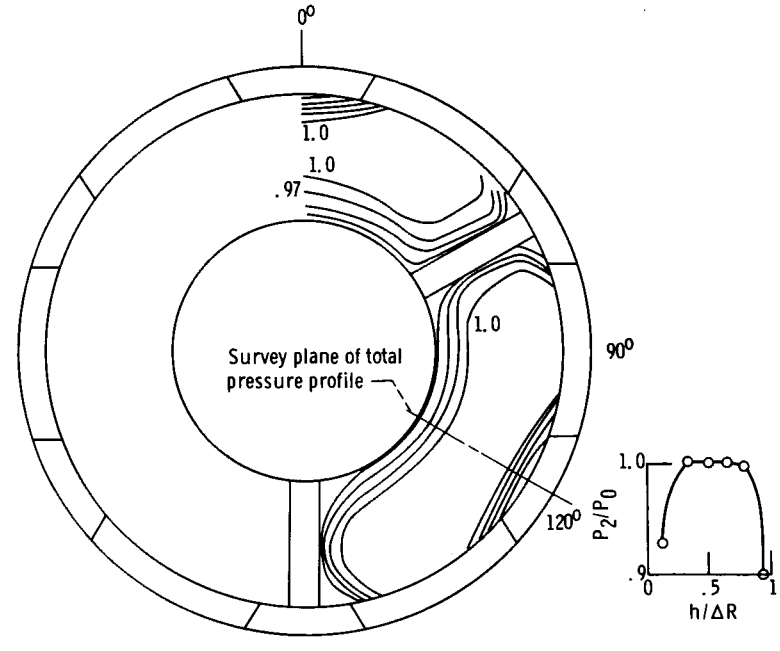

(d) Mach number, $M_0 = 0.8$; 10° multiple flap doors. Bypass mass flow ratio, $m_{bp}/m_0 = 0.127$; average total pressure recovery, $\bar{P}_2/P_0 = 0.982$; mass flow ratio, $m_3/m_0 = 0.653$; pressure ratio, $(P_{max} - P_{min})/\bar{P}_2 = 0.111$.

Figure 12. - Concluded.

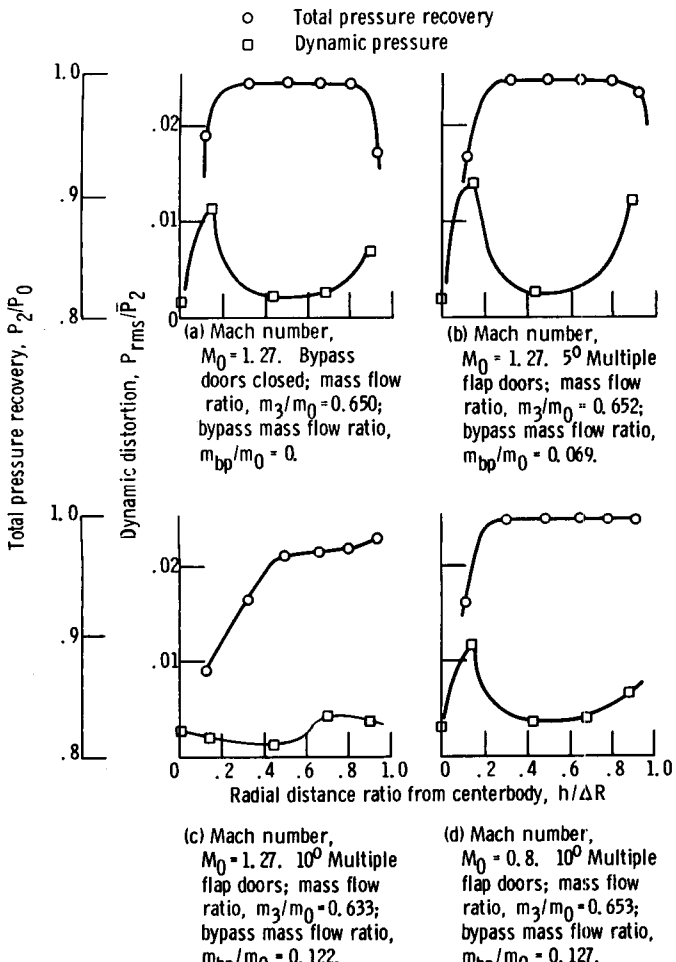

Figure 13. - Comparison of dynamic distortion with total pressure recoveries at compressor face station of 60-40 T inlet at design corrected weight flow.

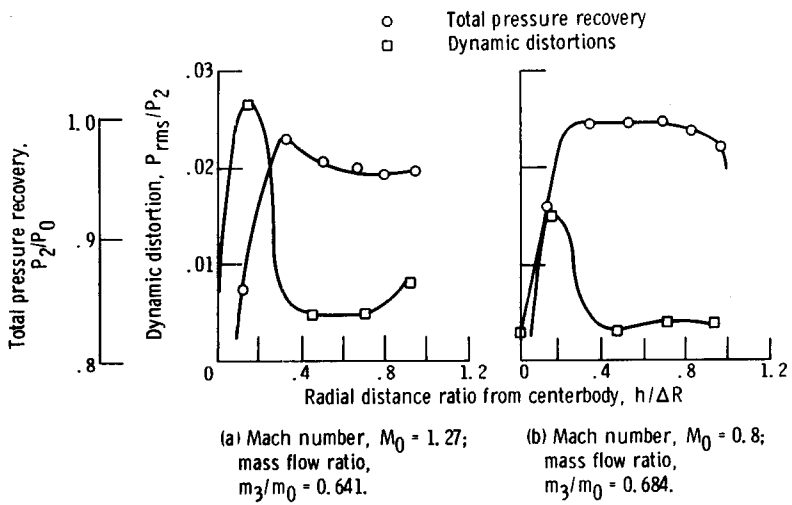

Figure 14. - Comparison of dynamic distortion with pressure recoveries at compresser face station of 60-40 T inlet. Engine mass flow greater than design; rms values for data of figure 15.

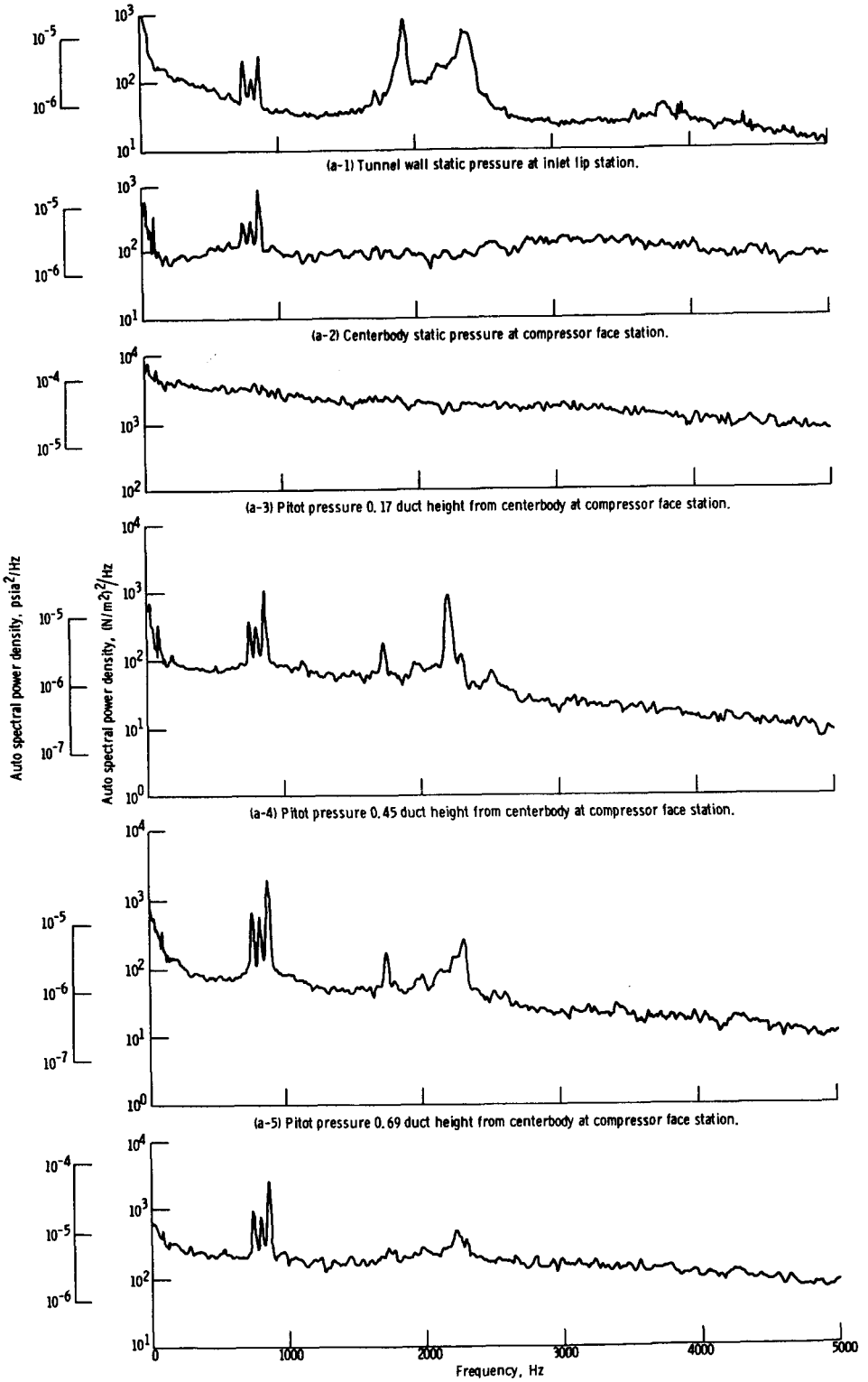

(a-1) Tunnel wall static pressure at inlet lip station.

(a-2) Centerbody static pressure at compressor face station.

(a-3) Pitot pressure 0.17 duct height from centerbody at compressor face station.

(a-4) Pitot pressure 0.45 duct height from centerbody at compressor face station.

(a-5) Pitot pressure 0.69 duct height from centerbody at compressor face station.

(a-6) Pitot pressure 0.89 duct height from centerbody at compressor face station.

(a) Mach number, M_0 = 1.27.

Figure 15. - Autospectral power density traces. 60-40 T inlet with 10^0 multiple flap bypass doors; rms data for these in figure 14.

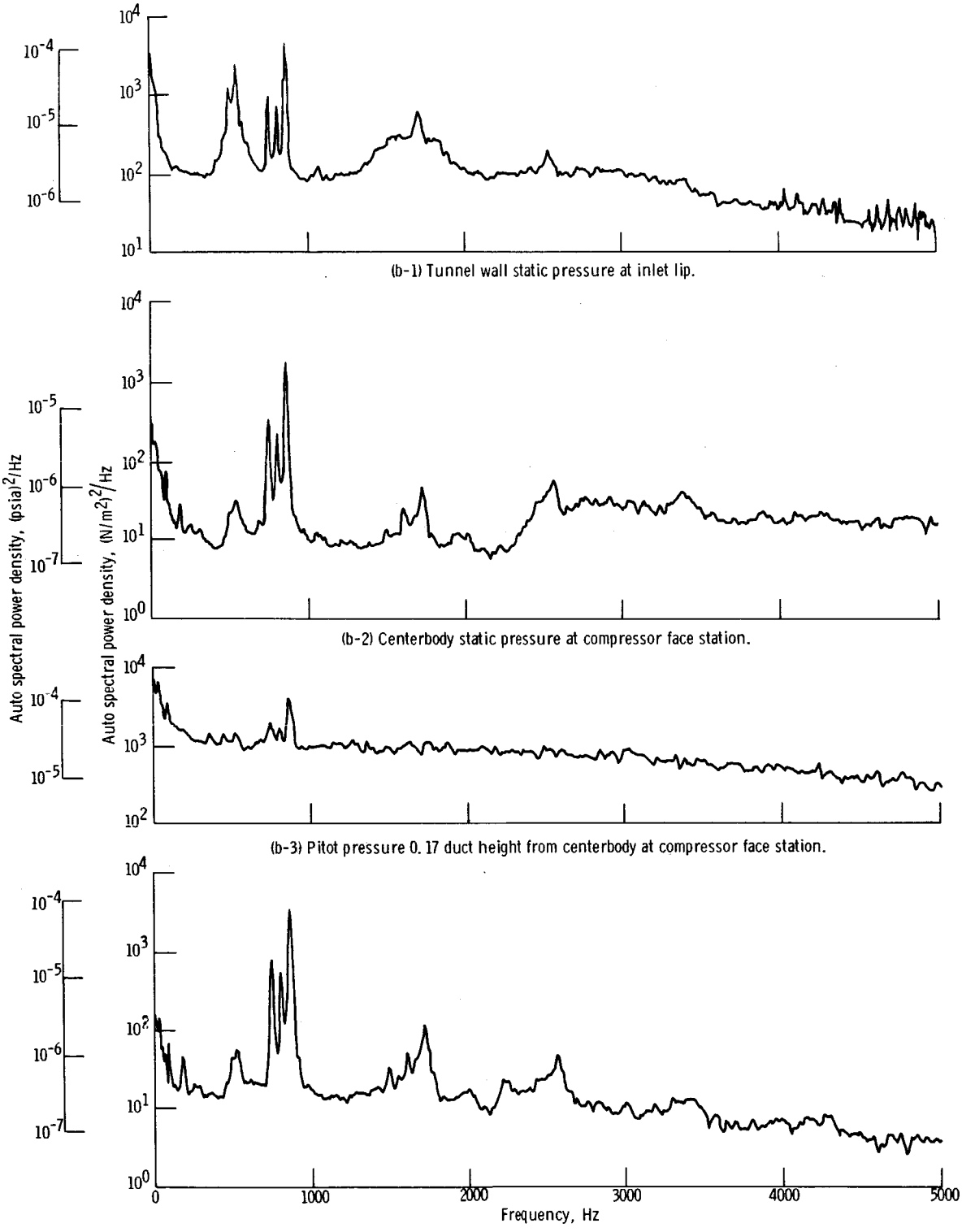

(b-1) Tunnel wall static pressure at inlet lip.

(b-2) Centerbody static pressure at compressor face station.

(b-3) Pitot pressure 0.17 duct height from centerbody at compressor face station.

(b-4) Pitot pressure 0.45 duct height from centerbody at compressor face station.

(b) Mach number, $M_0 = 0.8$.

Figure 15. - Continued.

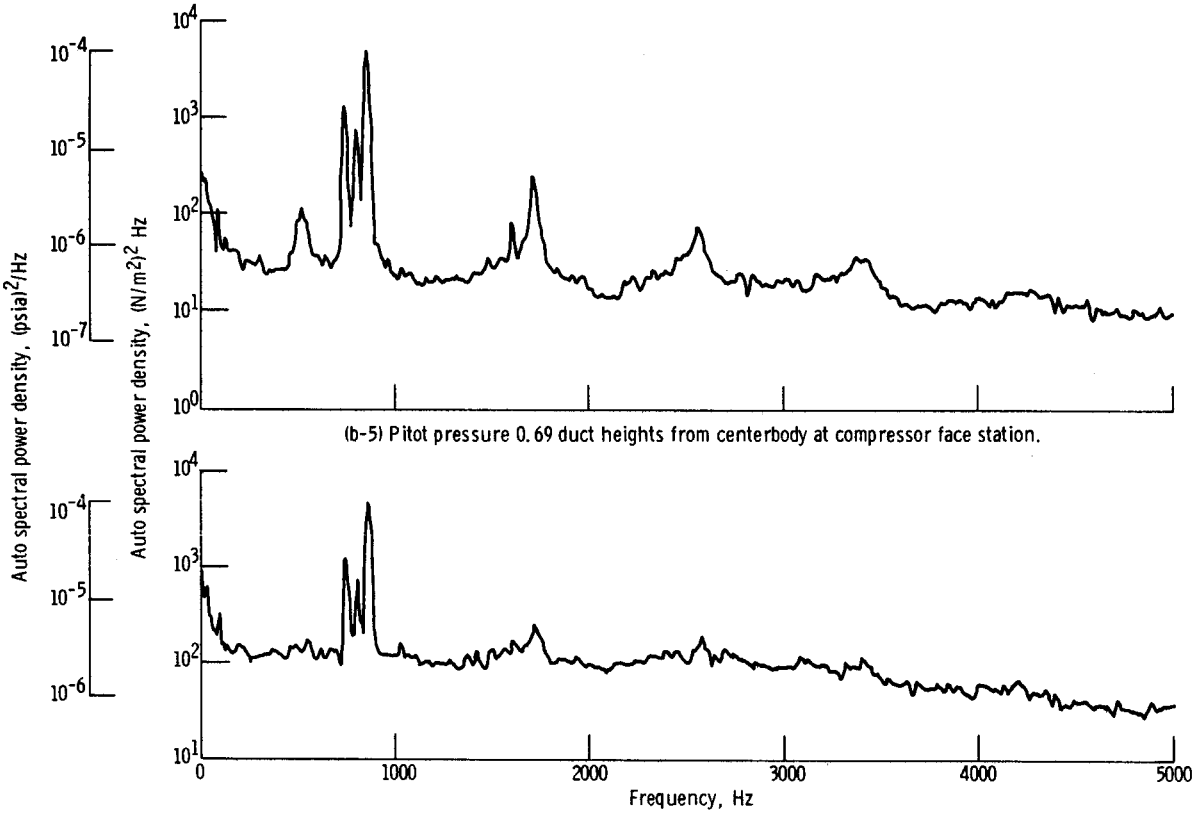

(b-5) Pitot pressure 0.69 duct heights from centerbody at compressor face station.

(b-6) Pitot pressure 0.89 duct height from centerbody at compressor face station.

(b) Concluded. Mach number, $M_0 = 0.8$.

Figure 15. - Concluded.

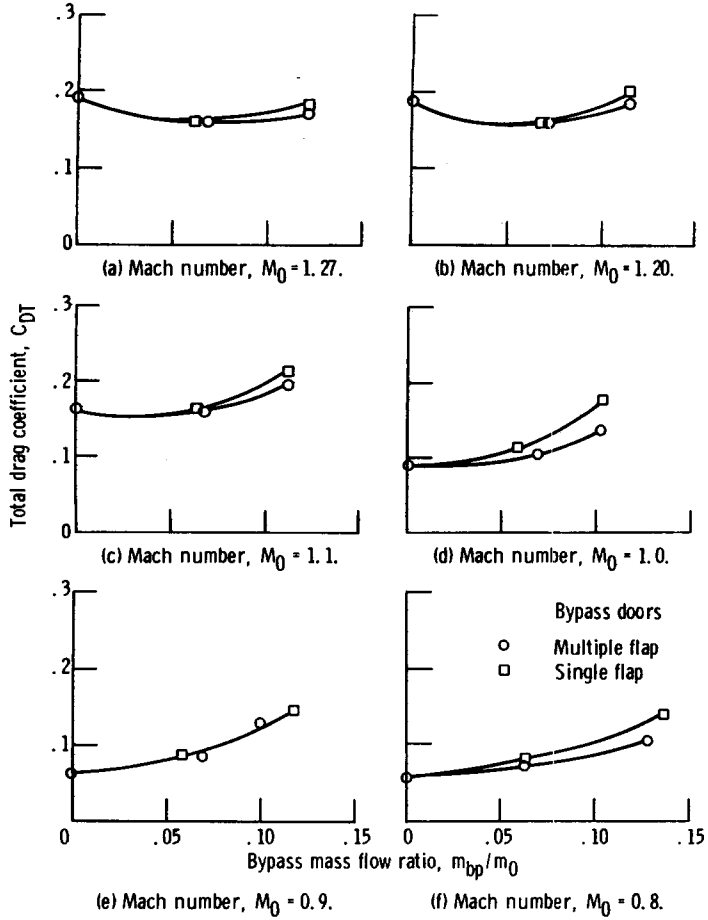

Figure 16. - Variation of total drag coefficient of transonic 60-40 T inlet with bypass mass flow ratio at design corrected weight flow.

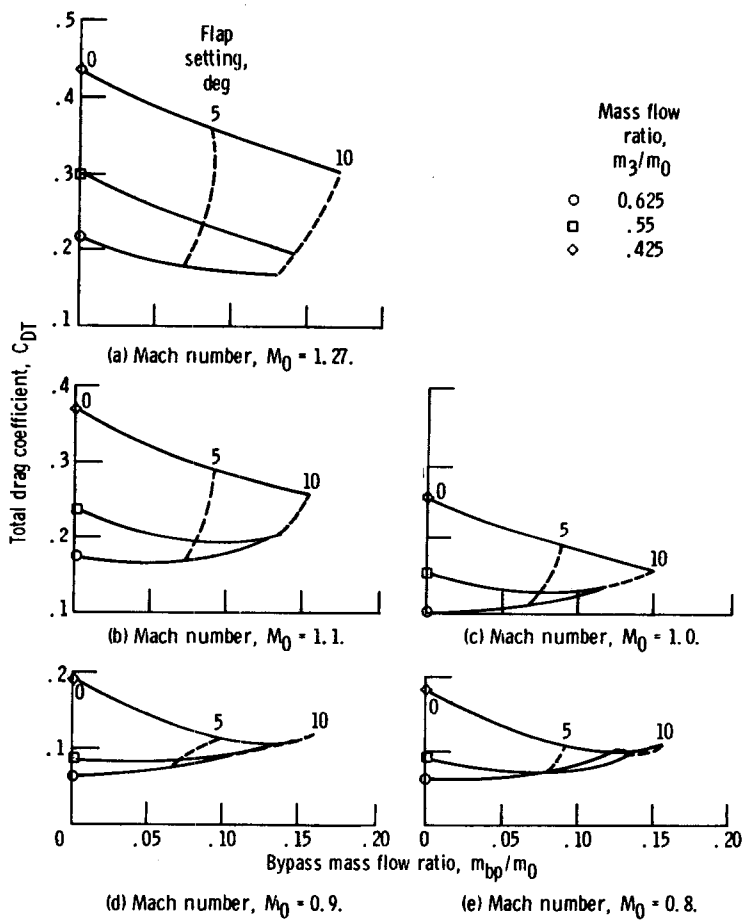

Figure 17. - Total drag coefficient of 60-40 T inlet as function of bypass spillage at various compressor face mass flows.

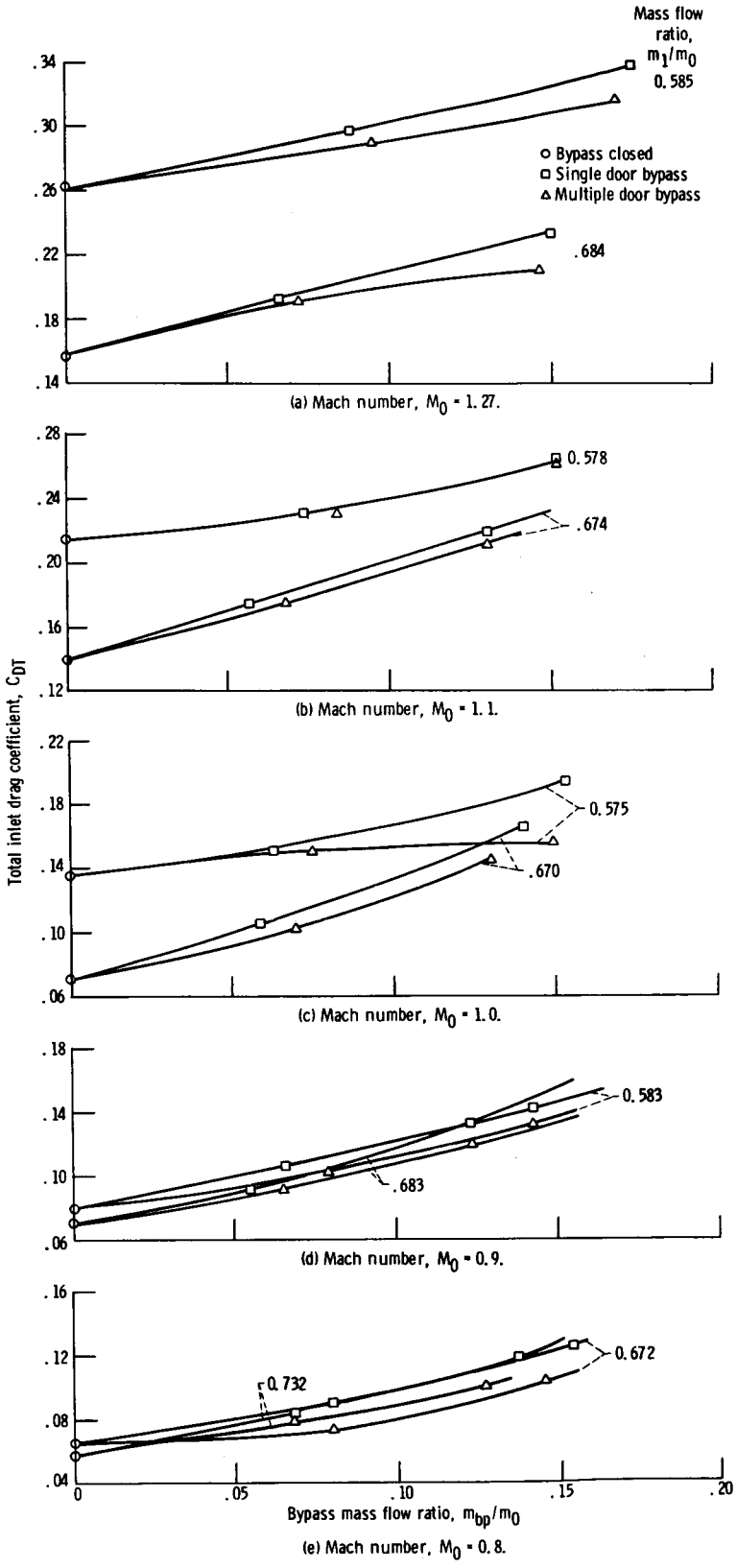

Figure 18. - Total inlet drag coefficient as function of bypass mass flow ratio 60-40 T inlet.

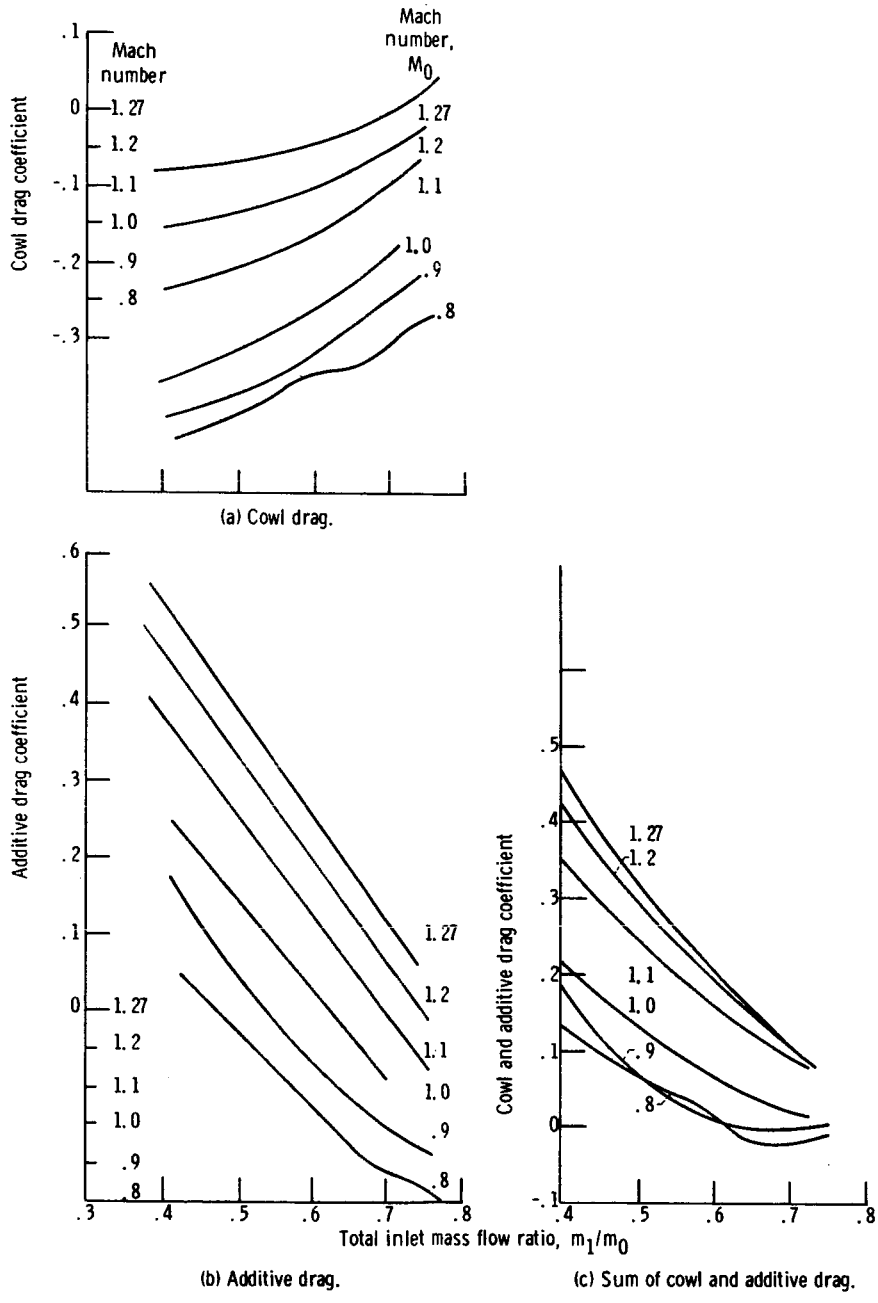

Figure 19. - Cowl and additive drag coefficients of 60-40 T inlet at various Mach numbers. To assume a particular Mach number curve, shift the drag coefficient scale so that its zero is opposite the desired Mach number mark.

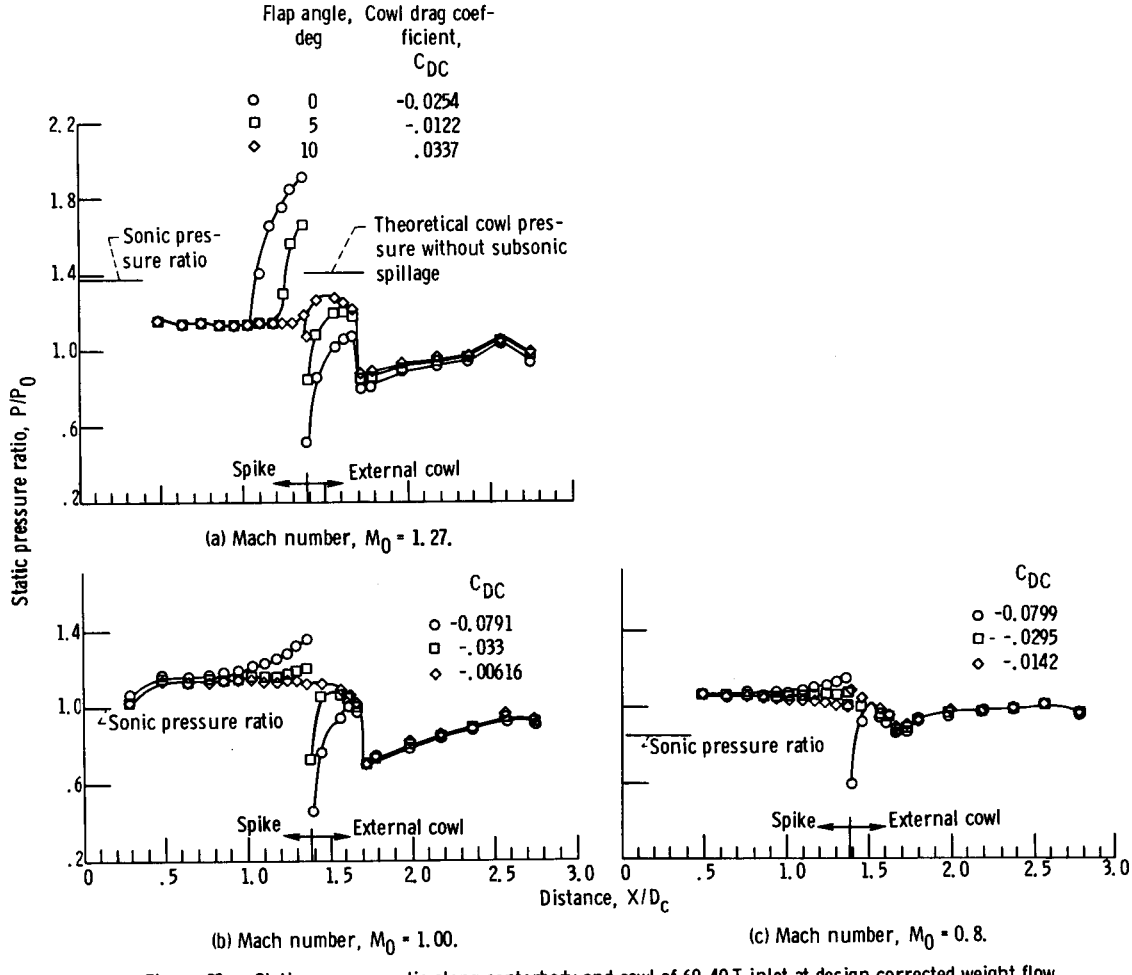

(a) Mach number, $M_0 = 1.27$.

(b) Mach number, $M_0 = 1.00$.

(c) Mach number, $M_0 = 0.8$.

Figure 20. - Static pressure ratio along centerbody and cowl of 60-40 T inlet at design corrected weight flow.

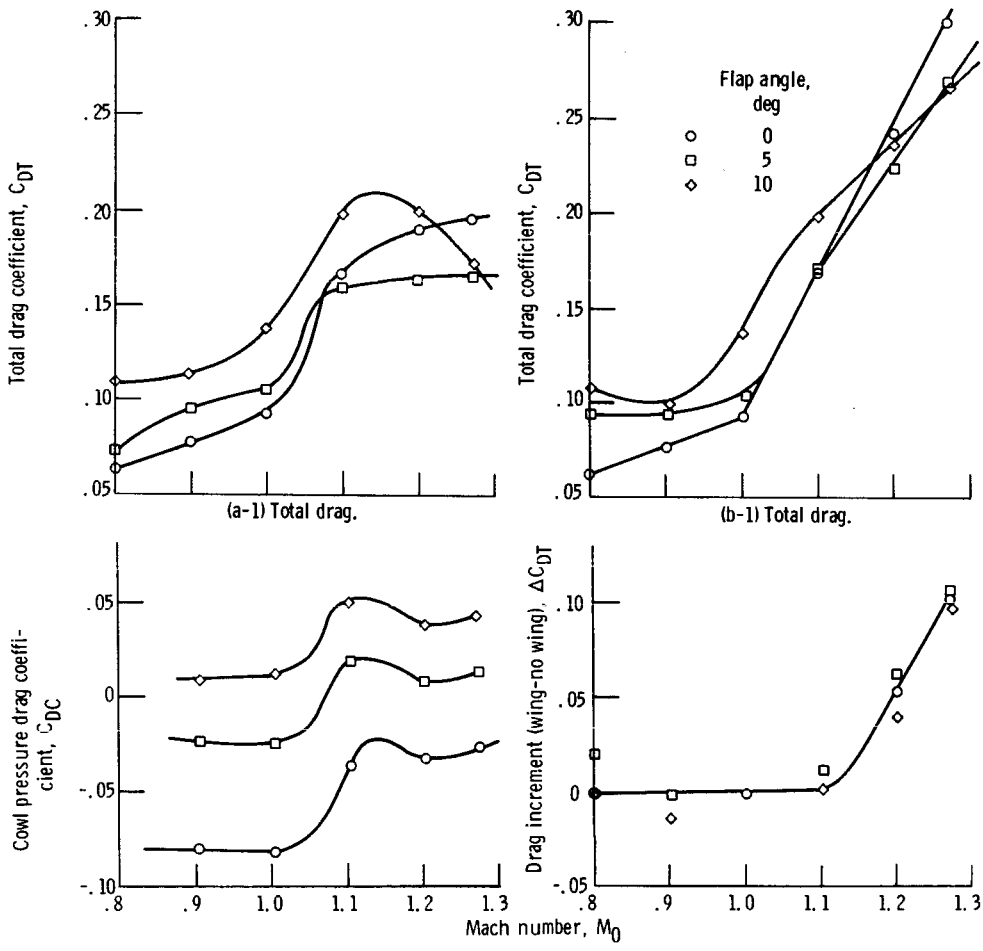

Figure 21. - Drag coefficient as function of Mach number for 60-40 T inlet with multiple flap bypass at design connected weight flow.

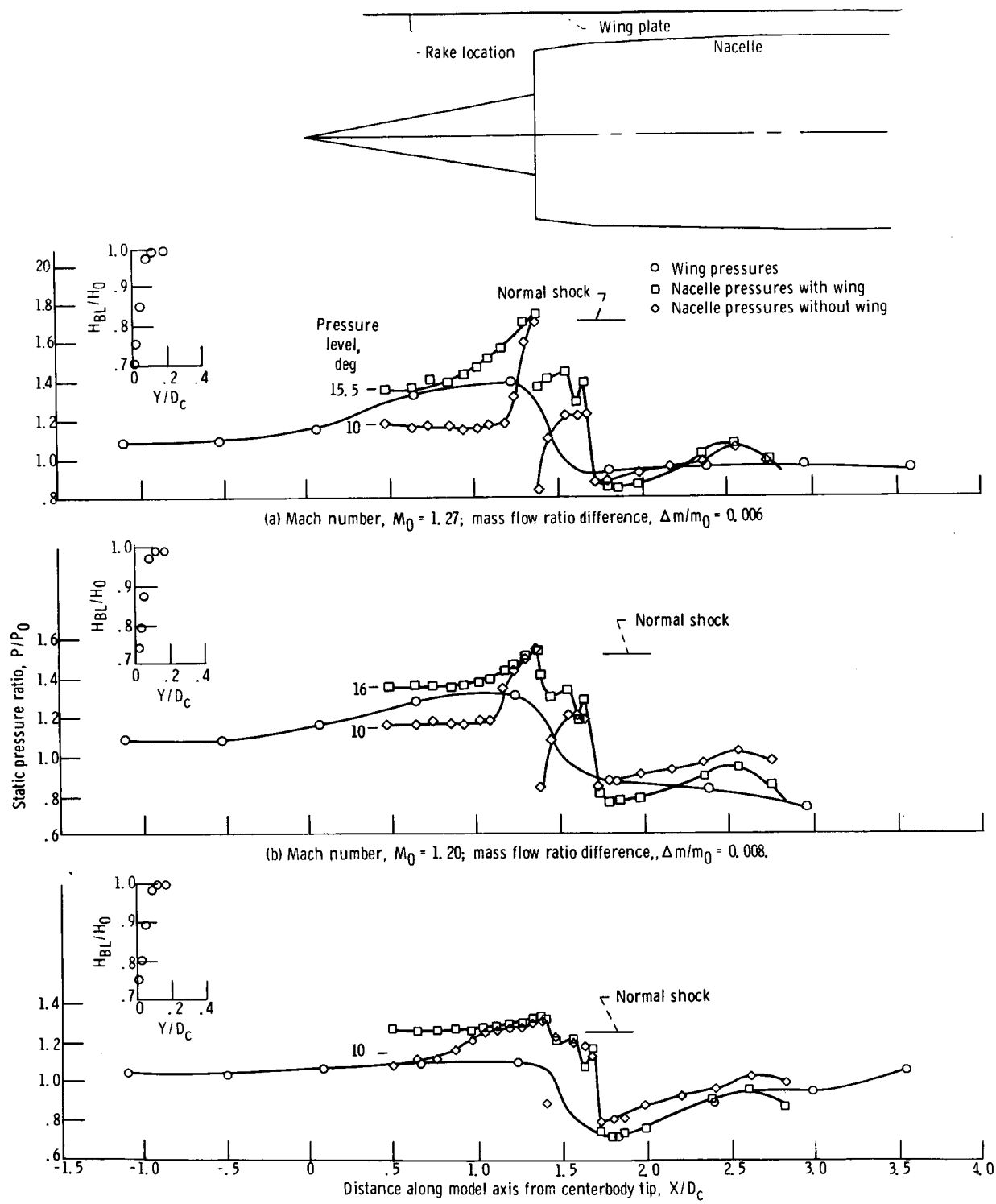

(a) Mach number, $M_0 = 1.27$; mass flow ratio difference, $\Delta m/m_0 = 0.006$

(b) Mach number, $M_0 = 1.20$; mass flow ratio difference,, $\Delta m/m_0 = 0.008$.

(c) Mach number, $M_0 = 1.1$; mass flow ratio difference, $\Delta m/m_0 = 0.014$

Figure 22. - Effect of wing on nacelle external static pressure for 60-40 T inlet with 5^0 multiple flap bypass doors.

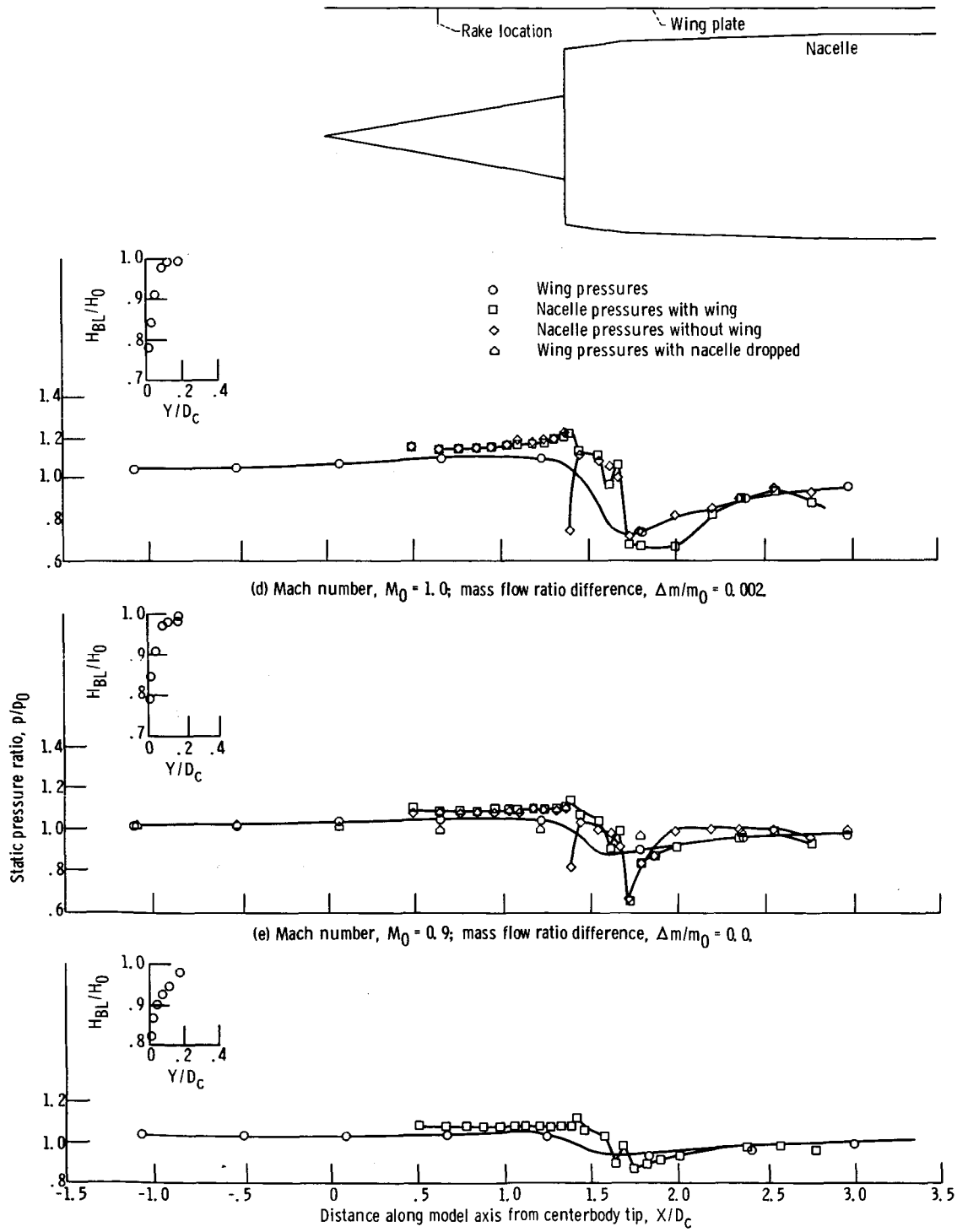

(d) Mach number, $M_0 = 1.0$; mass flow ratio difference, $\Delta m/m_0 = 0.002$.

(e) Mach number, $M_0 = 0.9$; mass flow ratio difference, $\Delta m/m_0 = 0.0$.

(f) Mach number, $M_0 = 0.8$; mass flow ratio difference, $\Delta m/m_0 = 0.005$.

Figure 22. - Concluded.

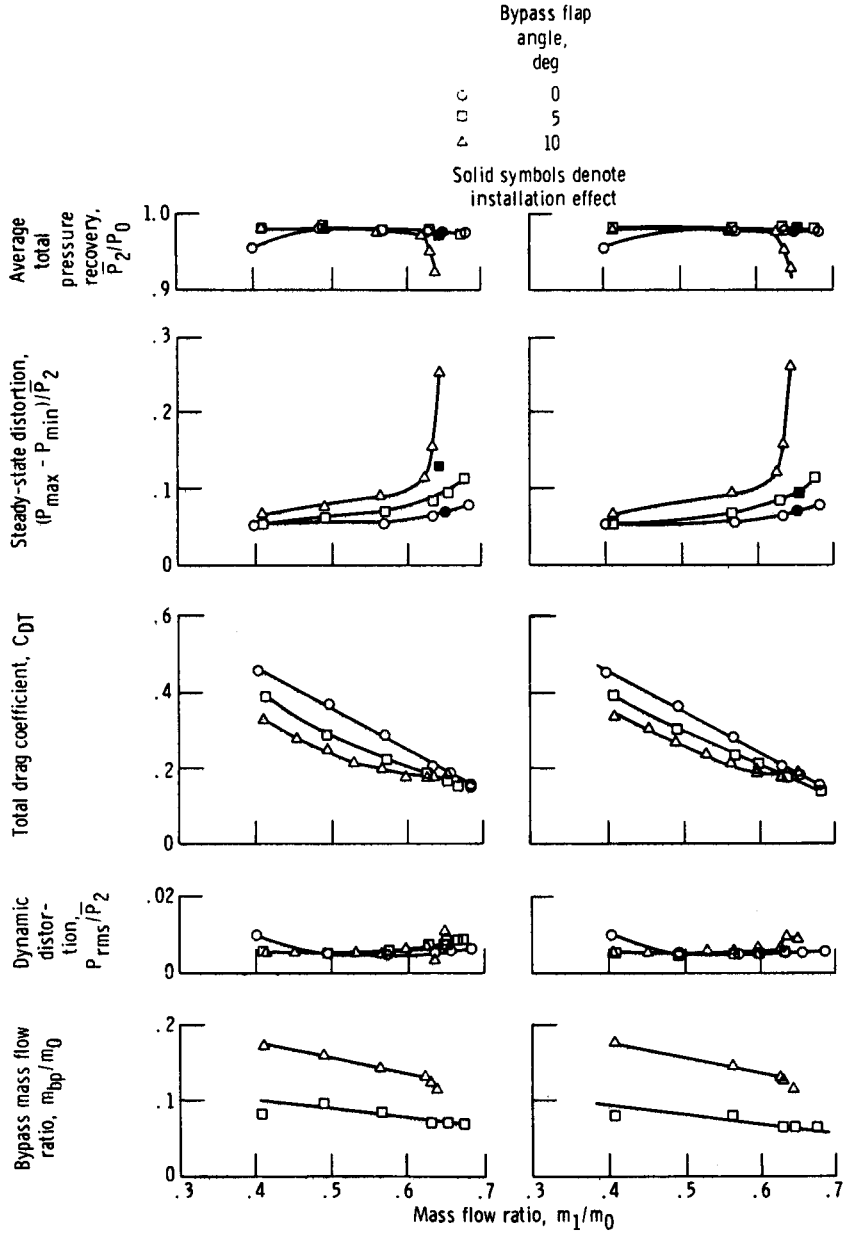

(a-1) Multiple flap bypass doors. (a-2) Single flap bypass doors.

(a) Mach number, $M_0 = 1.27$.

Figure 23. - General performance of 60-40 T inlet.

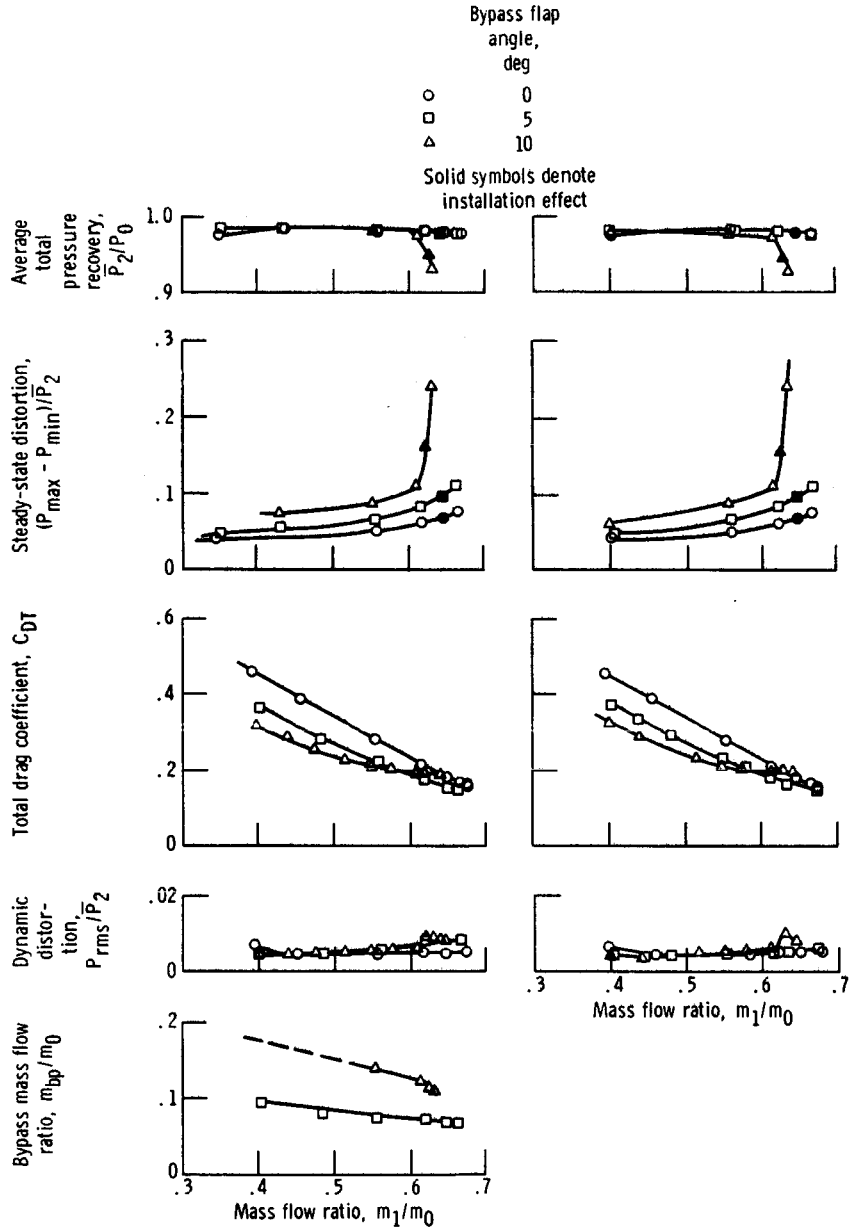

(b-1) Multiple flap bypass doors. (b-2) Single flap bypass doors.

(b) Mach number, M_0 = 1.20.

Figure 23. - Continued.

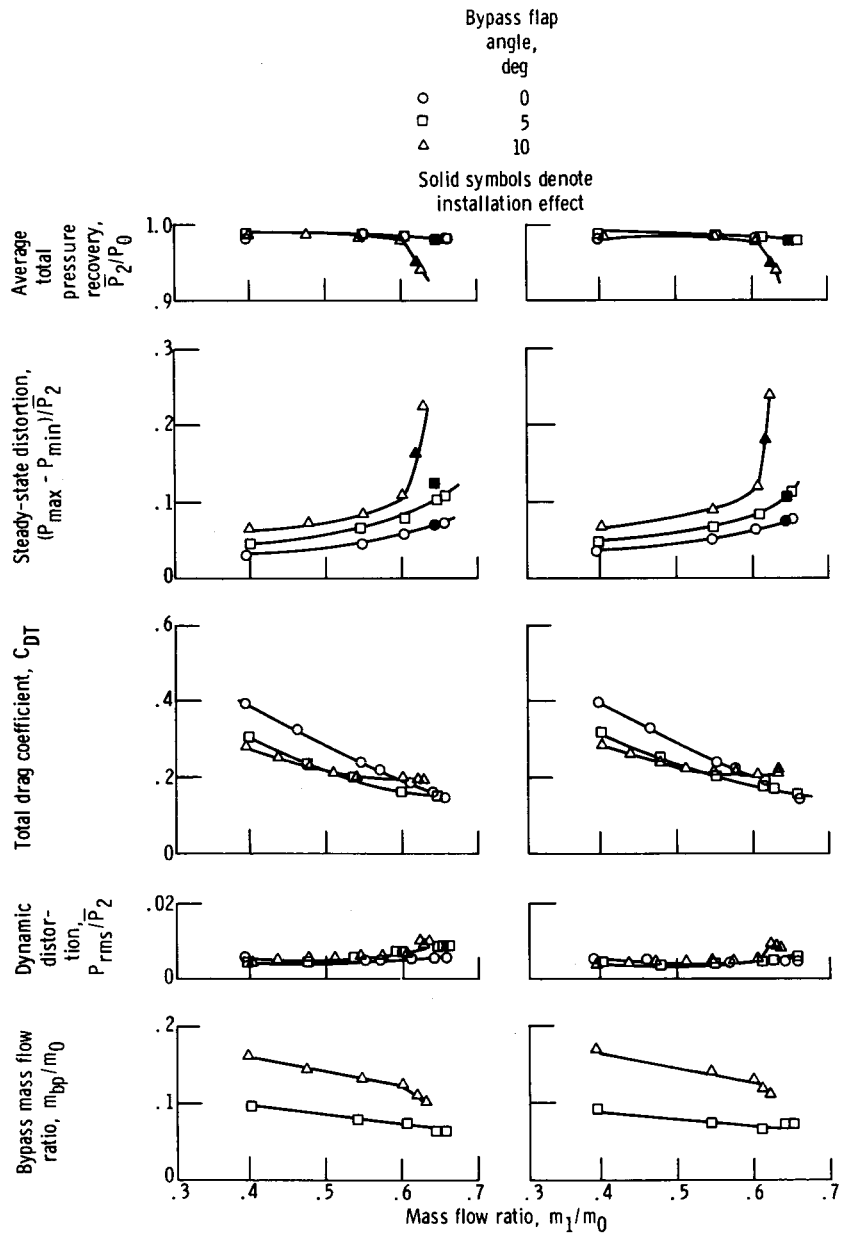

(c-1) Multiple flap bypass doors. (c-2) Single flap bypass doors.

(c) Mach number, $M_0 = 1.1$.

Figure 23. - Continued.

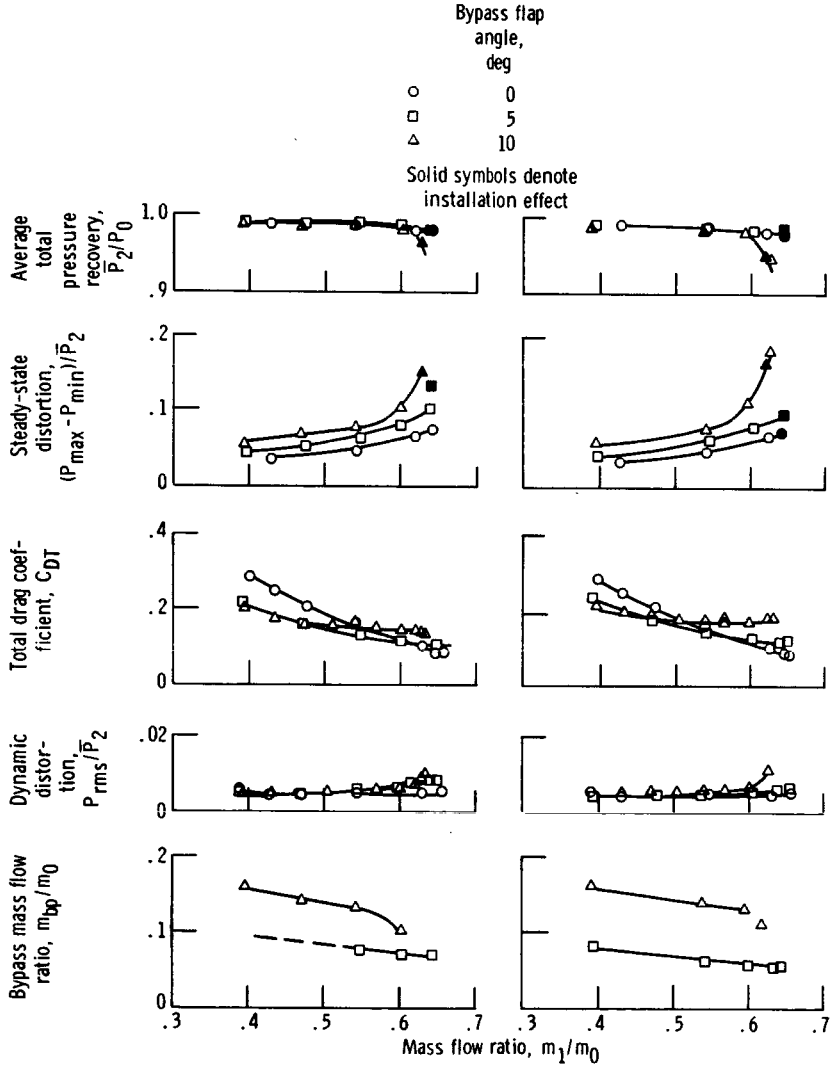

(d-1) Multiple flap bypass doors. (d-2) Single flap bypass doors.

(d) Mach number, $M_0 = 1.0$.

Figure 23. - Continued.

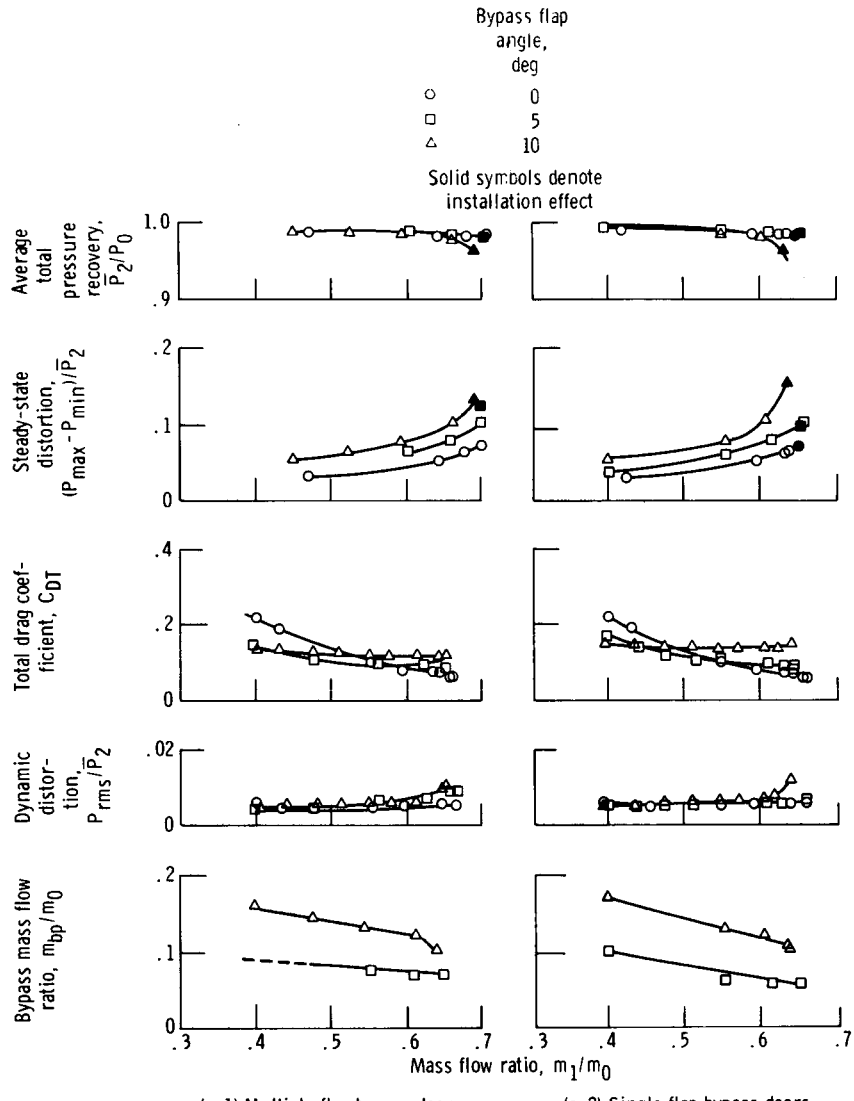

(e-1) Multiple flap bypass doors. (e-2) Single flap bypass doors.

(e) Mach number, $M_0 = 0.9$.

Figure 23. - Continued.

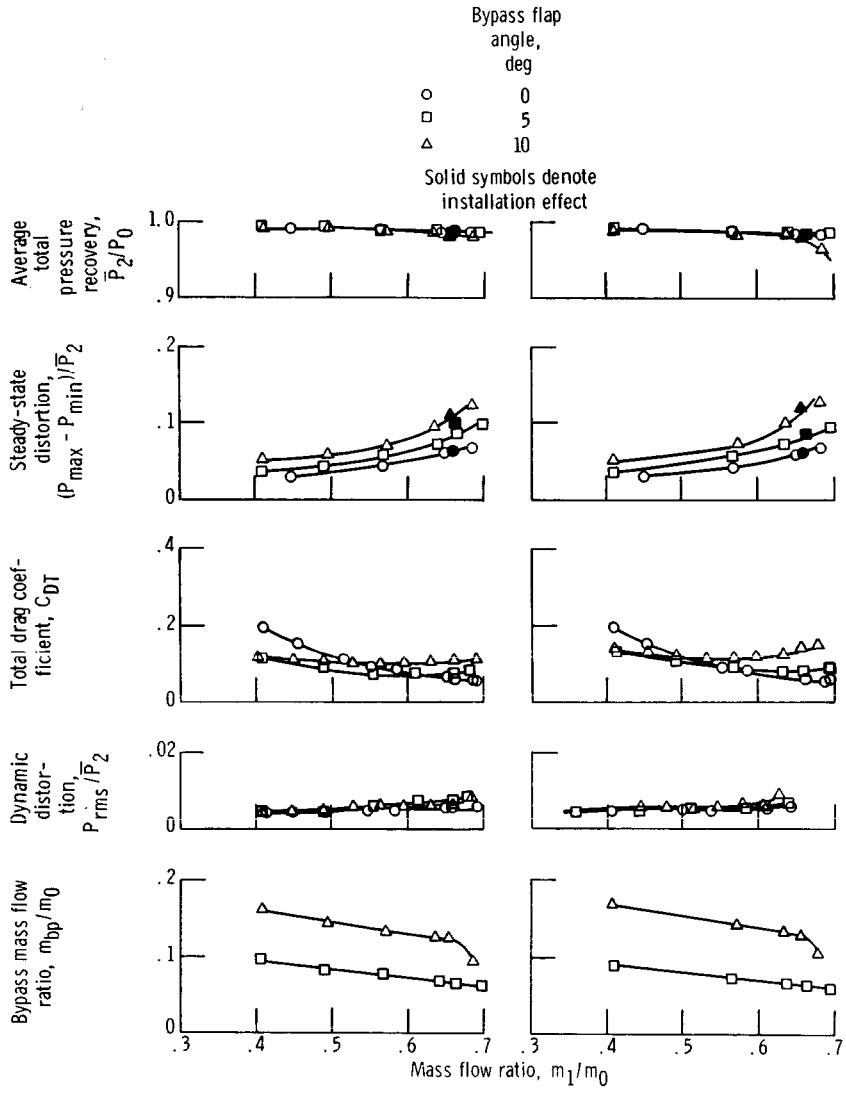

(f-1) Multiple flap bypass doors. (f-2) Single flap bypass doors.

(f) Mach number, $M_0 = 0.8$.

Figure 23. - Concluded.

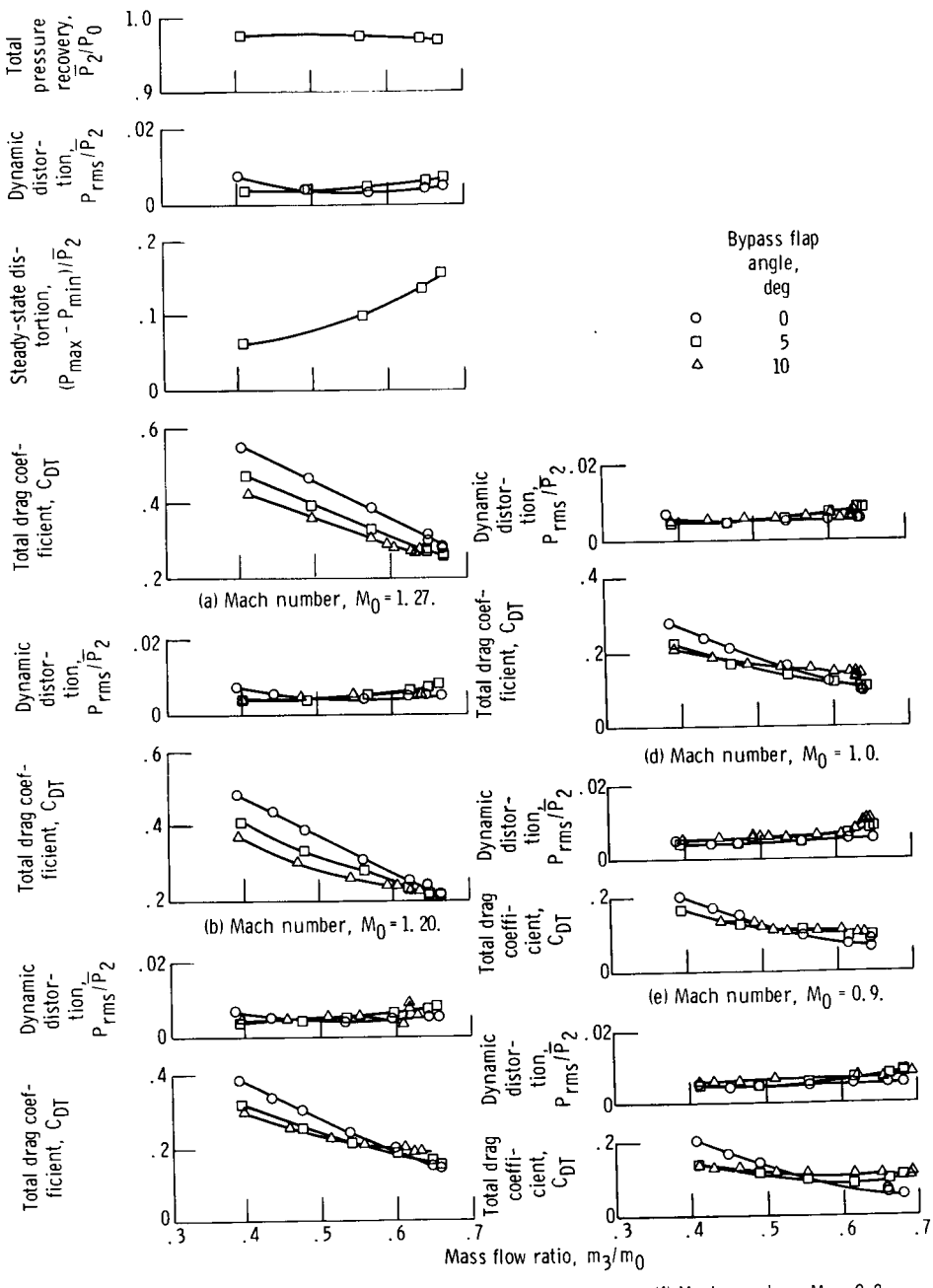

Figure 24. - General inlet performance of 60-40 T inlet mounted under simulated wing.

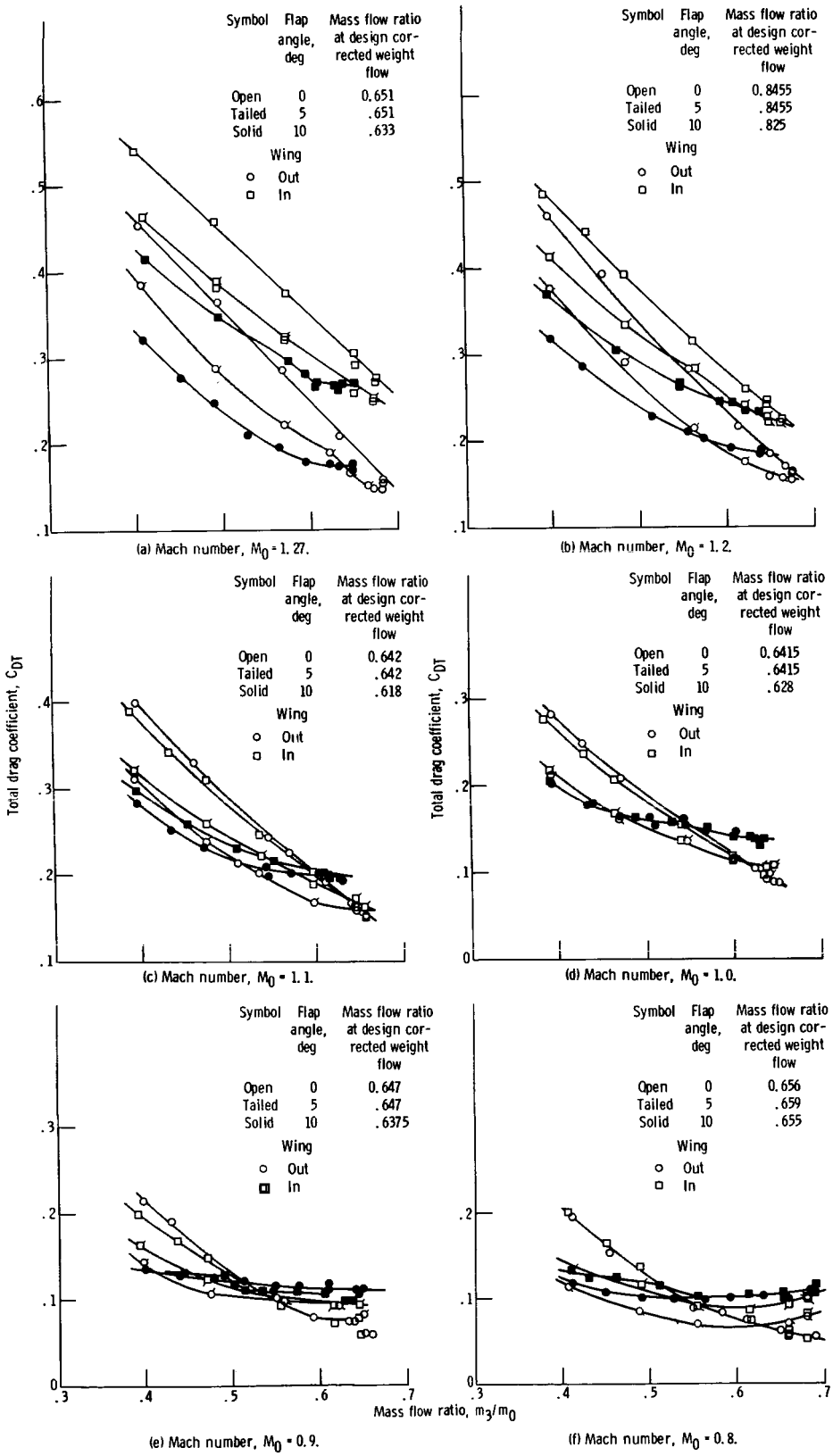

(a) Mach number, $M_0 = 1.27$.

(b) Mach number, $M_0 = 1.2$.

(c) Mach number, $M_0 = 1.1$.

(d) Mach number, $M_0 = 1.0$.

(e) Mach number, $M_0 = 0.9$.

(f) Mach number, $M_0 = 0.8$.

Figure 25. - Effect of wing on total drag coefficient of 60-40 T inlet with multiple bypass doors.